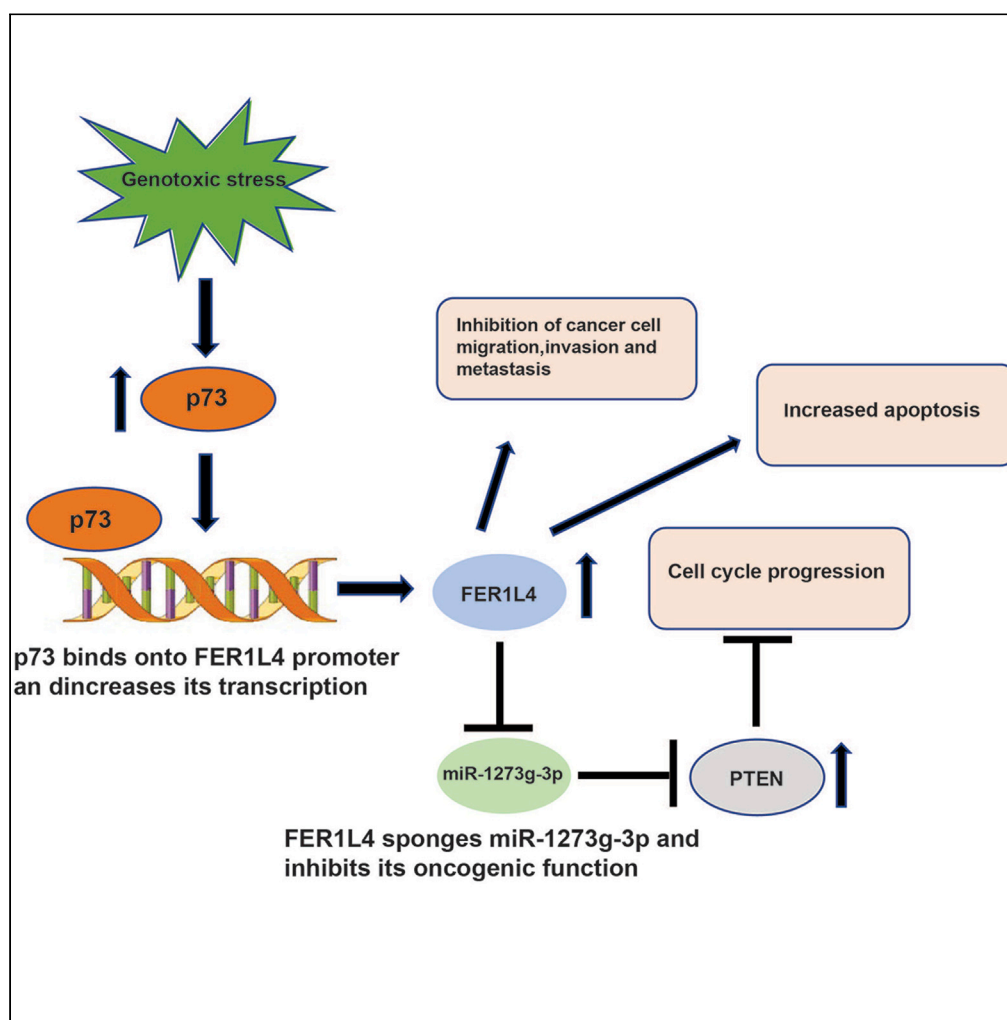Article

p73-regulated FER1L4 lncRNA sponges the oncogenic potential of miR-1273g-3p and aids in the suppression of colorectal cancer metastasis

Apoorva Uboveja, Yatendra Kumar Satija, Fouzia Siraj, Daman Saluja

dsalujach1959@gmail.com (D.S.)
yksatija@gmail.com (Y.K.S.)

Highlights

Long non-coding RNA FER1L4 functions as a direct transcriptional target of p73

FER1L4 plays a pivotal role in p73-mediated cell-cycle arrest and apoptosis

FER1L4kd augments colorectal cancer cell proliferation in a p73-dependent manner

p73-FER1L4 axis sponges miR-1273g-3p and inhibits its oncogenic role

Article

p73-regulated FER1L4 lncRNA sponges the oncogenic potential of miR-1273g-3p and aids in the suppression of colorectal cancer metastasis

Apoorva Uboveja,[1,4] Yatendra Kumar Satija,[1,3,*] Fouzia Siraj,[2] and Daman Saluja[1,5,*]

SUMMARY

p73 belongs to the p53 tumor suppressor family and is involved in the suppression of metastasis. However, its specific mechanism of action remains to be elucidated. Long non-coding RNAs portray a crucial role in tumor suppression. We have identified lncRNA FER1L4 as a p73 transcriptional target. The binding of p73 to FER1L4 promoter was established by bioinformatics analysis, luciferase reporter, and ChIP assays. Both FER1L4 and p73 knockdown enhanced the migration and invasion rate of colorectal cancer cells. FER1L4 also plays a critical role in p73-mediated cell-cycle arrest and apoptosis. FER1L4 sponged the expression of miR-1273g-3p, which, in turn, increased PTEN expression, leading to cell-cycle arrest. RNA *in situ* hybridization revealed the down-regulation of both p73 and FER1L4 expression in a metastatic colon cancer tissue as compared with non-metastatic tissue. Collectively, we impart conclusive proof that p73 exerts its anti-metastatic properties by inducing lncRNA FER1L4 in response to genotoxic stress.

INTRODUCTION

Non-coding RNAs do not possess protein-coding properties but function as important regulatory transcripts in biological processes. These consist of transfer RNAs (tRNAs), microRNAs (miRNAs), ribosomal RNAs (rRNAs), small nucleolar RNAs (snoRNAs), and long non-coding RNAs (lncRNAs) (Struhl, 2007). LncRNAs are usually more than 200 nucleotides in length and lack an open reading frame encoding a protein, and they differ from any known class of non-coding RNA (Wapinski and Chang, 2011). LncRNAs control gene expression at various levels that encompass transcriptional, post-transcriptional, and translational modulation (Batista and Chang, 2013; Fernandes et al., 2019; Geisler and Coller, 2013; Rinn and Chang, 2012; Xu et al., 2014). A mounting number of studies reveal that lncRNAs portray pivotal roles in tumorigenesis and may be utilized in the diagnosis of cancers (Chen et al., 2014; Geisler and Coller, 2013; Naz et al., 2021; Xu et al., 2014). Various studies demonstrate that the deregulated lncRNAs have a major role in the pathogenesis of many human cancers, such as bladder cancer, colorectal cancer, gastric cancer, breast cancer, and esophageal cancer (;Li et al., 2014; Shao et al., 2014; Tang et al., 2013). However, the attributes and roles of lncRNAs in tumorigenesis have remained chiefly obscure. It is of utmost importance to explore novel lncRNAs as biomarkers for therapeutic intervention.

p73 belongs to the p53 tumor suppressor pedigree and plays an important role in tumor suppression (Dötsch et al., 2010; Jost et al., 1997; Melino et al., 2002; Yoon et al., 2015). The significance of p73 in tumor suppression is accentuated by the observation that p73 knockout mice are extremely susceptible to unconstrained tumor development. As a result of its vigorous anti-proliferative function, p73 is maintained at low quantities in unstressed cells. Under genotoxic stress, p73 binds to its target genes and restrains cell proliferation by activating cell-cycle arrest and apoptosis followed by senescence. The p73 gene generates several isoforms by using its extrinsic (P1) or an alternative intrinsic (P2) promoter (Logotheti et al., 2013). The mechanisms of function of p73 isoforms stretch past those of a quintessential transcription factor and hold paramount significance. It is well known that TAp73 isoforms are tumor suppressive, whereas the N-terminal-lacking isoforms exert oncogenic properties (Stiewe et al., 2002). We have also recently confirmed the anti-metastatic role of p73 through the regulation of Navigator-3, a microtubule-binding protein (Uboveja et al., 2020). Taken together, p73 circuits can impose functional redundancy to p53 pathways as they administer different methods of reinstating flawed p53-regulated

[1]Dr.B.R. Ambedkar Centre for Biomedical Research and Delhi School of Public Health, University of Delhi, New Delhi 110007, India

[2]National Institute of Pathology (ICMR), Safdarjung Hospital Campus, New Delhi 110029, India

[3]Present address: CSIR-Indian Institute of Toxicology Research, Lucknow 226001, India

[4]Present address: UPMC Hillman Cancer Center, University of Pittsburgh School of Medicine, Pittsburgh, Pennsylvania, USA

[5]Lead contact

*Correspondence: dsalujach1959@gmail.com (D.S.), yksatija@gmail.com (Y.K.S.) https://doi.org/10.1016/j.isci.2022.103811

mechanisms in cancer cells. Nevertheless, escalating evidence indicates that these familiar p73 target genes may not be totally accountable for mediating p73 function in tumor suppression. Hence, elucidating novel p73 target genes are of paramount importance for the extensive interpretation of how p73 wields its tumor suppressive function.

Even though the literature on the p73 transcriptional circuit chiefly concentrates on protein-coding genes, it has been progressively pointed out that p73 is also able to transcriptionally modulate non-coding RNA (ncRNA) members. These involve microRNAs (miRNAs) and many p53-regulated long non-coding RNAs (lncRNAs). Diverse miRNAs have been empirically pinpointed to interact with p73 in cancer circuits. For instance, miR193A is known to be a direct p73 transcriptional target and miR193A inhibition reinstates p73-mediated cisplatin responsiveness in chemo-resistant tumors such as squamous cell carcinomas and osteosarcomas (Jacques et al., 2016; Ory et al., 2011). miR-323 is another p73-inhibiting miRNA, which can suppress p73 and accentuate prostate cancer growth and docetaxel resistance (Gao and Zheng, 2018). Analogous to miR-323, miR-1180 induces p73 to curb apoptosis in Wilms' tumors (Jiang et al., 2018). However, no study has been carried out to explore lncRNAs as possible targets of p73 transcriptional regulation. The current understanding of lncRNAs is rather restricted as compared with protein-coding genes. Nevertheless, mounting observations indicate that lncRNAs may serve as chief regulatory molecules that regulate gene expression in an array of human diseases, including cancer (Huarte, 2015; Liu et al., 2014; Yoon et al., 2013).

Fer-1-like family member 4 (FER1L4) lncRNA is a pseudogene and located on chromosome 20 in humans. It does not possess protein-coding capabilities but, instead, produces a 6,717-bp ncRNA that is majorly expressed in embryonic and adult tissues. It has been reported that lncRNA FER1L4 is down-regulated in gastric cancer (Xia et al., 2015), hepatocellular carcinoma (Wu et al., 2017), colon cancer (Yue et al., 2015), and endometrial carcinoma (Qiao and Li, 2016) and functions as a tumor suppressor in these cancers. In endometrial carcinoma, lncRNA FER1L4 suppresses cell proliferative ability and cell cycle via targeting PTEN (Qiao and Li, 2016). In glioblastoma, lncRNA FER1L4 is up-regulated and controls the glioma cells tumorigenicity (Ding et al., 2017). LncRNA FER1L4 can predict prognosis in hepatocellular carcinoma (Wu et al., 2017). However, the clinical importance and biological function of FER1L4 in colon cancer are still uncertain and need to be probed further.

In this study, we report that long non-coding RNA FER1L4 functions as a direct p73 transcriptional target and is up-regulated under genotoxic distress in a p73-dependent manner. The discovery of p73-binding sites in the FER1L4 promoter region pinpoints that FER1L4 expression is under direct regulation by p73, which was further established by chromatin immunoprecipitation (ChIP) and site-directed mutagenesis experiments. LncRNA FER1L4 also plays a chief role in p73-mediated cell-cycle arrest and apoptosis, as revealed by cell cycle analysis and Annexin-V/PI and TUNEL apoptosis assays. FER1L4 knockdown augments cell proliferation, migration, and invasion in a p73-dependent manner. We provide evidence that FER1L4 sponges miR-1273g-3p, thus inhibiting its oncogenic role. Furthermore, RNA *in situ* hybridization (RNA-ISH) performed in non-metastatic and metastatic human colon cancer tissue samples confirms that FER1L4 and p73 levels are significantly down-regulated in metastatic samples as compared with non-metastatic tumor tissue samples. Collectively, our findings provide strong evidence that lncRNA FER1L4 serves as a key player in mediating tumor suppressive function of p73.

RESULTS

Genotoxic stress enhances FER1L4 mRNA expression in a p73-regulated manner

In our previous paper (Uboveja et al., 2020), we have demonstrated that p73 expression levels are enhanced as a result of genotoxic stress caused by etoposide treatment (20 μM, 24 h) and doxorubicin (10 μM, 24 h) in HCT116p53$^{-/-}$p73$^{+/+}$ cell line and H1299p53$^{-/-}$ cell line. In order to determine the role of p73 in the modulation of FER1L4 levels, a quantitative real-time PCR was performed in HCT116p53$^{-/-}$ colorectal cancer cell line using etoposide (20 μM) as a cause of genotoxic distress. Etoposide treatment caused a significant up-regulation of FER1L4 mRNA levels as compared with untreated cells (Figure 1A). To further correlate the expression of FER1L4 mRNA with that of p73, we overexpressed p73 in HCT116p53$^{-/-}$ cells by transfection with a p73 overexpression plasmid. We observed enhanced FER1L4 mRNA levels in cells overexpressing p73 as compared with control cells transfected with empty plasmid (Figure 1A). To further investigate whether p73 levels are enhanced by etoposide treatment in other p53$^{-/-}$ cell lines also , H1299p53$^{-/-}$ cells
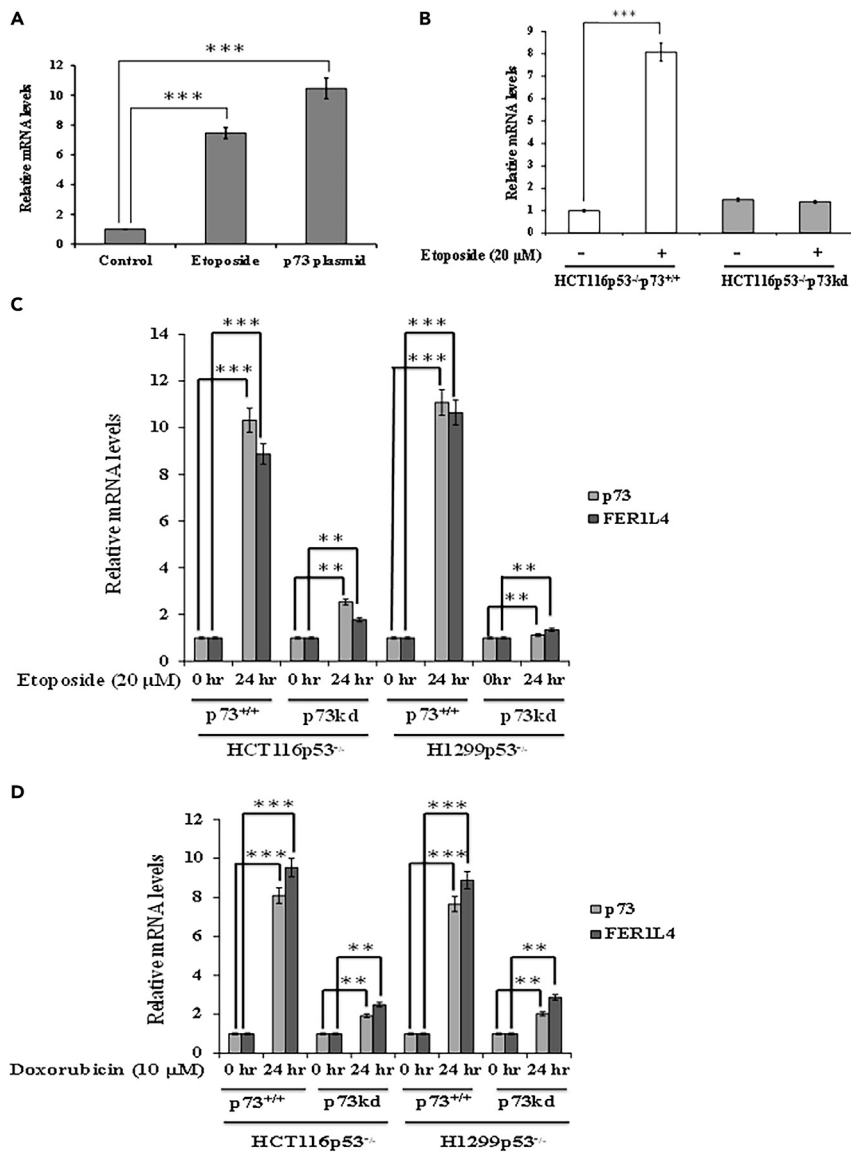
Figure 1. p73-mediated up-regulation of lncRNA FER1L4 under genotoxic stress

(A) HCT116p53$^{-/-}$p73$^{+/+}$ cells were subjected to etoposide (20 μM, 24 h) treatment or transfected with p73 plasmid (24 h) as indicated. Isolation of total RNA was carried out, and FER1L4 mRNA levels were quantified by qRT-PCR and normalized with β-actin. The results of three independent experiments are recorded as mean $\pm$ SD (unpaired two-tailed Student's t test, ***$p < 0.0001$)

(B) HCT116p53$^{-/-}$p73$^{+/+}$ (Control) and HCT116p53$^{-/-}$p73kd (p73kd) cells were subjected to etoposide treatment (20 μM, 24 h). Isolation of total RNA was carried out and FER1L4 mRNA levels were quantified by qRT-PCR and normalized with β-actin. The results of three independent experiments are recorded as mean $\pm$ SD (unpaired two-tailed Student's t test, ***$p < 0.0001$)

(C) RT-qPCR for p73 and FER1L4 in etoposide-treated (20 μM, 24 h) HCT116p53$^{-/-}$p73$^{+/+}$ and H1299p53$^{-/-}$ cells was carried out and normalized with β-actin. The results of three independent experiments are recorded as mean $\pm$ SD (unpaired two-tailed Student's t test, **$p < 0.01$, ***$p < 0.0001$)

(D) RT-qPCR for p73 and FER1L4 in doxorubicin-treated (10 μM, 24 h) HCT116p53$^{-/-}$p73$^{+/+}$ and H1299p53$^{-/-}$ cells was carried out and normalized with β-actin. The results of three independent experiments are recorded as mean $\pm$ SD (unpaired two-tailed Student's t test, **$p < 0.01$, ***$p < 0.0001$)

were exposed to etoposide (20 μM) treatment for 24 and 48 h and western blot analysis was carried out. An increase in p73 protein level was observed upon etoposide treatment in H1299p53$^{-/-}$ cells upto 48 h as compared with control cells (Figure S1A). FER1L4 mRNA levels were then checked in H1299p53$^{-/-}$ cells
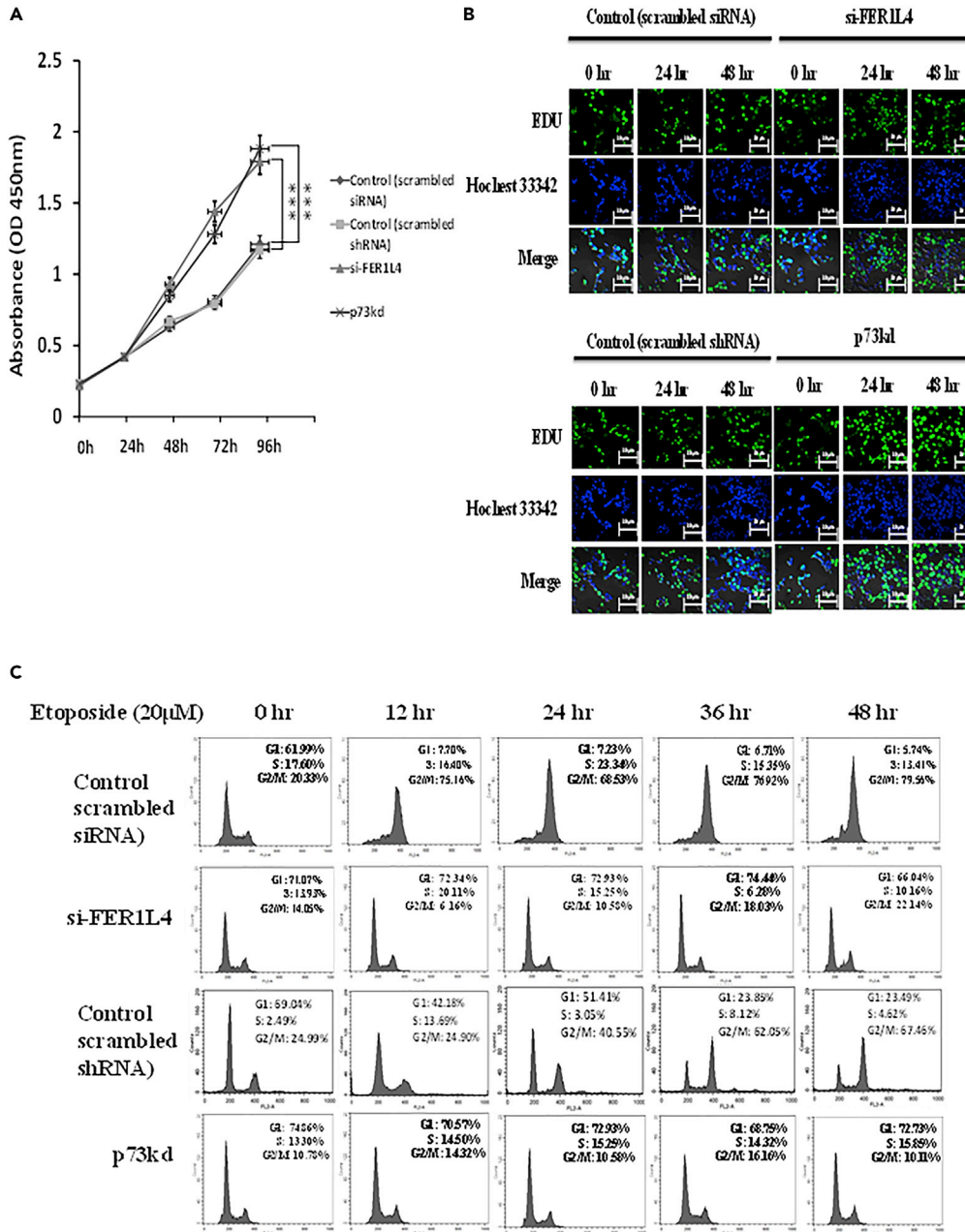
Figure 2. FER1L4kd enhances cell proliferation

(A) CCK-8 assays were conducted to measure the viability of HCT116p53$^{-/-}$p73$^{+/+}$ (Control – HCT116p53$^{-/-}$p73$^{+/+}$ cells transfected with scrambled siRNA), si-FER1L4 (FER1L4kd – HCT116p53$^{-/-}$p73$^{+/+}$ cells transfected with siRNA against FER1L4), HCT116p53$^{-/-}$p73$^{+/+}$ (Control – HCT116p53$^{-/-}$p73$^{+/+}$ cells transfected with scrambled shRNA), and HCT116p53$^{-/-}$p73kd (p73kd – HCT116p53$^{-/-}$p73$^{+/+}$ cells transfected with specific shRNA against p73) cells for the indicated time periods. The results of three independent experiments are recorded as mean $\pm$ SD (unpaired two-tailed Student's *t* test, ***$p < 0.0001$)

(B) EdU staining assays were conducted to compare the proliferation rates of HCT116p53$^{-/-}$p73$^{+/+}$ (Control – HCT116p53$^{-/-}$p73$^{+/+}$ cells transfected with scrambled siRNA), si-FER1L4 (FER1L4kd – HCT116p53$^{-/-}$p73$^{+/+}$ cells transfected with siRNA against FER1L4), HCT116p53$^{-/-}$p73$^{+/+}$ (Control – HCT116p53$^{-/-}$p73$^{+/+}$ cells transfected with scrambled shRNA), and HCT116p53$^{-/-}$p73kd (p73kd – HCT116p53$^{-/-}$p73$^{+/+}$ cells transfected with specific shRNA against p73) cells. The data presented are representative of three independent experiments

(C) HCT116p53$^{-/-}$p73$^{+/+}$ (Control – HCT116p53$^{-/-}$p73$^{+/+}$ cells transfected with scrambled siRNA), si-FER1L4 (FER1L4kd – HCT116p53$^{-/-}$p73$^{+/+}$ cells transfected with siRNA against FER1L4), HCT116p53$^{-/-}$p73$^{+/+}$ (Control –

Figure 2. *Continued*

HCT116p53$^{-/-}$p73$^{+/+}$ cells transfected with scrambled shRNA), and p73kd (HCT116p53$^{-/-}$p73$^{+/+}$ cells transfected with specific shRNA against p73) were subjected to etoposide treatment (20 μM) for the indicated time points. Cells were treated with propidium iodide and quantified by flow cytometry. The data presented are representative of three independent experiments.

treated with etoposide (20 μM, 24 h) and found to be significantly increased as compared with unstressed cells (Figure S1B). A stable p73 knockdown cell line was created using a specific shRNA in HCT116p53$^{-/-}$ cells and pooled puromycin-resistant population was selected. Knockdown was ascertained through western blotting (Figure S1C). Quantitative real-time PCR was carried out to check FER1L4 mRNA levels in etoposide-treated control and p73kd cells. p73kd resulted in abrogation of FER1L4 induction even when cells were treated with etoposide (Figure 1B). Moreover, we compared the kinetics of FER1L4 expression post etoposide treatment in Control and p73kd cells from 12 to 48 h. We observed that amplified expression of FER1L4 mRNA was noticed in control cells at 12 h and it kept on increasing with increase in the duration of genotoxic stress. However, the induction of FER1L4 was abrogated by p73kd. Hence, no increase was detected in FER1L4 mRNA levels even after exposure to genotoxic stress (Figure S1D). Similarly, a stable p73kd cell line (pooled puromycin-resistant population) was generated using a specific shRNA in H1299p53$^{-/-}$ cells. Knockdown was confirmed through western blotting (Figure S1E). FER1L4 expression levels were then checked in etoposide-treated (20 μM) H1299p53$^{-/-}$p73$^{+/+}$ and H1299p53$^{-/-}$p73kd cells and found to be significantly decreased in p73kd cells as compared with p73$^{+/+}$ cells (Figure 1C).

To further check whether p73 and FER1L4 levels get induced by other genotoxic drugs, HCT116p53$^{-/-}$p73$^{+/+}$, HCT116p53$^{-/-}$p73kd, H1299p53$^{-/-}$p73$^{+/+}$, and H1299p53$^{-/-}$p73kd cells were exposed to doxorubicin (10 μM) treatment for 24 h. p73 and FER1L4 expression was then checked by quantitative real-time PCR. The expression of both the genes was found to be significantly decreased in p73kd cells as compared with p73$^{+/+}$ cells upon doxorubicin treatment upto 24 h (Figure 1D). Collectively, our results demonstrate that p73 expression is a prerequisite for increase in FER1L4 expression.

In our literature survey, we came across lncRNA MALAT1, which is known to play a crucial role in cancer cell progression and tumorigenesis. We wanted to check whether MALAT1 is also regulated by p73 in a similar manner as FER1L4 lncRNA. In this direction, we conducted a qPCR to check the expression levels of p73, FER1L4, and MALAT1 in HCT116p53$^{-/-}$p73$^{+/+}$, HCT116p53$^{-/-}$p73kd, H1299p53$^{-/-}$p73$^{+/+}$, and H1299p53$^{-/-}$p73kd cells. Our results clearly demonstrated that FER1L4 expression levels decreased significantly in p73kd cells as compared with p73wt cells (Figure S1F). However, MALAT1 expression levels remained unchanged in both p73wt and p73kd cells, indicating that MALAT1 lncRNA is not regulated by p73. To further delineate whether p53 also plays a role in FER1L4 regulation, specific shRNA was used to abrogate p73 expression in HCT116p53$^{+/+}$ cells (control cell line) and pooled puromycin-resistant population was selected. Knockdown of p73 was confirmed by western blotting (Figure S1G). FER1L4 mRNA levels in control and p73kd cells subjected to etoposide treatment were measured by quantitative real-time PCR. FER1L4 mRNA levels were observed to be notably decreased in p73kd cells even when p53 is present (Figure S1H), indicating that p53 protein does not alter FER1L4 expression levels.

FER1L4 suppresses colorectal cancer cell proliferation

To ascertain the role of FER1L4 in cell proliferation, its expression was down-regulated by transfecting HCT116p53$^{-/-}$p73$^{+/+}$ cells with siRNA targeting FER1L4 (si-FER1L4). After 24 h, we evaluated the silencing efficiency under genotoxic stress (20 μM) by quantitative real-time PCR (Figure S2A) and QuantiGene ViewRNA fluorescent RNA-ISH (Figure S2B), and the results demonstrated that FER1L4 expression was significantly lower in the si-FER1L4 groups as compared with the control group (HCT116p53$^{-/-}$p73$^{+/+}$ cells transfected with scrambled siRNA). We further carried out a CCK-8 assay to investigate the role of FER1L4 in cell proliferation. Cell growth curves revealed that down-regulating FER1L4 expression in HCT116p53$^{-/-}$p73$^{+/+}$ cells by using specific siRNA against FER1L4 notably increased cell growth as compared with the control cells (HCT116p53$^{-/-}$p73$^{+/+}$ cells transfected with scrambled siRNA) (Figure 2A). Also, p73kd (HCT116p53$^{-/-}$p73$^{+/+}$ cells transfected with specific shRNA against p73) cells followed a similar trend and increased cell growth as compared with the control cells (HCT116p53$^{-/-}$p73$^{+/+}$ cells transfected with scrambled shRNA) (Figure 2A). 5-Ethynyl-2′-deoxyuridine (EdU) staining was carried out to further confirm the anti-proliferative ability of FER1L4, and the results demonstrated
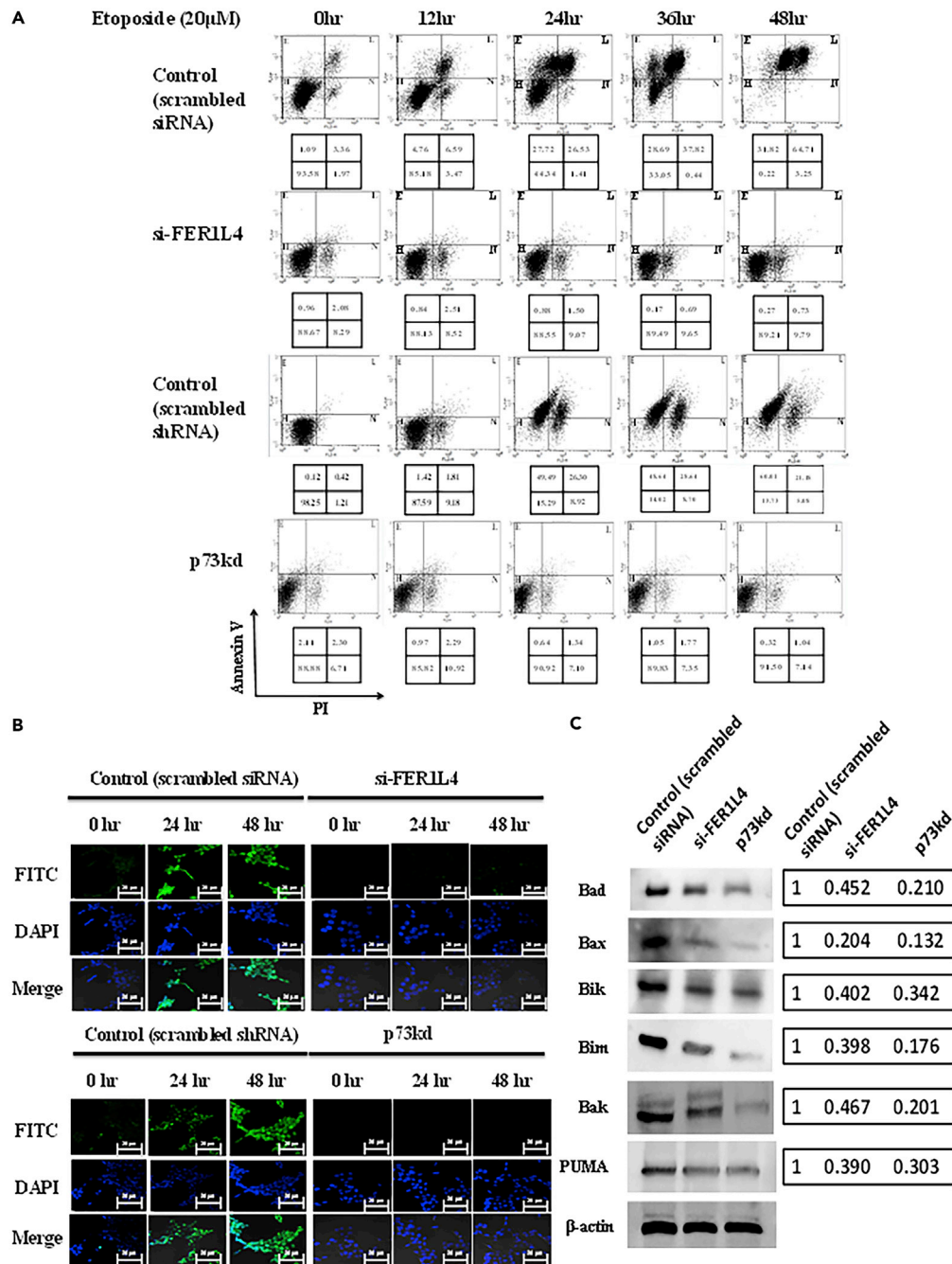
Figure 3. FER1L4 portrays a critical role in p73-mediated apoptosis

(A) Annexin-V/PI apoptosis assay was performed in etoposide-treated (20 μM; 12, 24, 36, 48 h) HCT116p53$^{-/-}$p73$^{+/+}$ (Control – HCT116p53$^{-/-}$p73$^{+/+}$ cells transfected with scrambled siRNA), si-FER1L4 (FER1L4kd – HCT116p53$^{-/-}$p73$^{+/+}$ cells transfected with siRNA against FER1L4), HCT116p53$^{-/-}$p73$^{+/+}$ (Control – HCT116p53$^{-/-}$p73$^{+/+}$ cells transfected with scrambled shRNA), and HCT116p53$^{-/-}$p73kd (p73kd – HCT116p53$^{-/-}$p73$^{+/+}$ cells transfected with specific shRNA against p73) cells. H, Healthy; E, early apoptotic; L, late apoptotic; N, necrotic cells. The data presented are representative of three independent experiments

(B) TUNEL staining was conducted to assess the apoptotic rates of etoposide-treated (20 μM, 24 h) HCT116p53$^{-/-}$p73$^{+/+}$ (Control – HCT116p53$^{-/-}$p73$^{+/+}$ cells transfected with scrambled siRNA), si-FER1L4 (FER1L4kd – HCT116p53$^{-/-}$p73$^{+/+}$ cells transfected with siRNA against FER1L4), HCT116p53$^{-/-}$p73$^{+/+}$ (Control – HCT116p53$^{-/-}$p73$^{+/+}$ cells transfected with scrambled shRNA), and HCT116p53$^{-/-}$p7kd (p73kd – HCT116p53$^{-/-}$p73$^{+/+}$ cells transfected with specific shRNA against p73) cells. The data presented are representative of three independent experiments

Figure 3. *Continued*

(C) Cell lysates from HCT116p53$^{-/-}$p73$^{+/+}$ (Control – HCT116p53$^{-/-}$p73$^{+/+}$ cells transfected with scrambled siRNA), FER1L4kd (HCT116p53$^{-/-}$p73$^{+/+}$ cells transfected with siRNA against FER1L4), and p73kd (HCT116p53$^{-/-}$p73$^{+/+}$ cells transfected with specific shRNA against p73) cells were collected and western blotting was conducted for the indicated proteins. β-Actin was taken as loading control. Densitometry analysis is also shown. The data presented are representative of three independent experiments

that there were higher number of EdU-positive cells in the si-FER1L4 group than in the control group (HCT116p53$^{-/-}$p73$^{+/+}$ cells transfected with scrambled siRNA) after 24 and 48 h of etoposide treatment (Figures 2B and S3A). p73kd (HCT116p53$^{-/-}$p73$^{+/+}$ cells transfected with specific shRNA against p73) cells also portrayed a higher number of EdU-positive cells than the control cells (HCT116p53$^{-/-}$p73$^{+/+}$ cells transfected with scrambled shRNA) (Figures 2B and S3A). Similarly, the cell cycle assay demonstrated that, in the presence of genotoxic stress, higher number of cells were arrested in G2/M phase in both the control groups (HCT116p53$^{-/-}$p73$^{+/+}$ cells transfected with scrambled siRNA and HCT116p53$^{-/-}$p73$^{+/+}$ cells transfected with scrambled shRNA). However, in the case of si-FER1L4 (HCT116p53$^{-/-}$p73$^{+/+}$ cells transfected with specific siRNA against FER1L4) and p73kd (HCT116p53$^{-/-}$p73$^{+/+}$ cells transfected with specific shRNA against p73) cells, there was no noteworthy cell-cycle arrest at any of the time points in the duration of genotoxic stress (Figures 2C and S3B), suggesting that FER1L4 lncRNA might play a significant role in p73-mediated suppression of proliferation of cells.

We further scrutinized the effect of FER1L4 on p73-mediated apoptosis. In this direction, HCT116p53$^{-/-}$p73$^{+/+}$ (Control – HCT116p53$^{-/-}$p73$^{+/+}$ cells transfected with scrambled siRNA), FER1L4kd (si-FER1L4 – HCT116p53$^{-/-}$p73$^{+/+}$ cells transfected with specific siRNA against FER1L4), HCT116p53$^{-/-}$p73$^{+/+}$ (Control – HCT116p53$^{-/-}$p73$^{+/+}$ cells transfected with scrambled shRNA), and p73kd (HCT116p53$^{-/-}$p73$^{+/+}$ cells transfected with specific shRNA against p73) cells were given genotoxic stress for indicated time points and flow cytometric assays were conducted. FER1L4kd and p73kd cells demonstrated reduced apoptosis as compared with the control cells upon genotoxic stress (Figures 3A and S4A). TUNEL staining further confirmed a marked decrease in the apoptotic population upon etoposide treatment in FER1L4kd and p73kd cells as compared with control cells (Figure 3B). In addition, the expression levels of pro-apoptotic markers such as Bad, Bax, Bik, Bim, BID, Bak, and PUMA were observed to be reduced in FER1L4kd and p73kd after etoposide treatment as compared with the control cells (Figures 3C and S4B). Taken together, these data demonstrate that FER1L4 portrays a significant part in p73-mediated activation of apoptosis.

Pinpointing putative p73-binding sites in the lncRNA FER1L4 promoter region

As our data indicate that FER1L4 is a p73-inducible gene and p73 originally acts as a transcription factor that induces its target DNA sequences, our next step was to check whether p73 interacts with the promoter of FER1L4. Hence, we scanned the human FER1L4 genomic region upstream and downstream of the Transcription Start Site (TSS) for prospective p73-binding sites by employing the TFBind software (tfbind.hgc.jp) and JASPAR database (jasper.genereg.net). One perfect p73-binding site comprises two 10-bp half-sites, 5′- RRRC(A/T)(A/T)GYYY, where C(A/T)(A/T)G acts as the core sequence with purine (R) and pyrimidine (Y) bases functioning as flanking sequences. The two half binding sites are separated by a spacer of upto 13 bases (Figure S5A). Fourteen presumed p73 half binding sites (BS) were observed in the upstream region (−4,002 bp) and nine sites were observed in the downstream region (+2,900 bp) with respect to the TSS (Figure S5B). In order to ascertain the binding of p73 with these prospective binding sites, the upstream region was further divided into three parts: U1 (−4,002 to −3,107; 896 bp), U2 (−2,539 to −1,825; 715 bp), and U3 (−1,680 to −844; 837 bp), and the downstream region was further divided into two parts: D1 (+1,092 to +1,691; 600 bp) and D2 (+2,116 to +2,900; 785 bp) (Figure S5C).

p73 directly interacts with FER1L4 promoter

To identify the functional p73-binding site located in FER1L4 promoter, five fragments that consist of these prospective p73-binding sites—U1, U2, U3, D1, and D2—were cloned upstream of a luciferase reporter gene in pGL4.2 firefly luciferase reporter vector. These different reporter constructs were then transfected into HCT116p53$^{-/-}$ cells along with pRL-TK, which acts as an internal loading control and encodes Renilla luciferase (Figure 4A). Luciferase activity was quantified post 48 h etoposide treatment. The empty pGL4.20 luciferase vector was utilized as a negative control. Reporter constructs carrying the U1 (−4,002 to −3,107) and U2 (−2,539 to −1,825) regions demonstrated notably higher luciferase activity under genotoxic stress as compared with the control (Figure 4B). In contrast, constructs carrying U3, D1, and D2 regions demonstrated negligible alteration in luciferase activity upon treatment with etoposide as compared
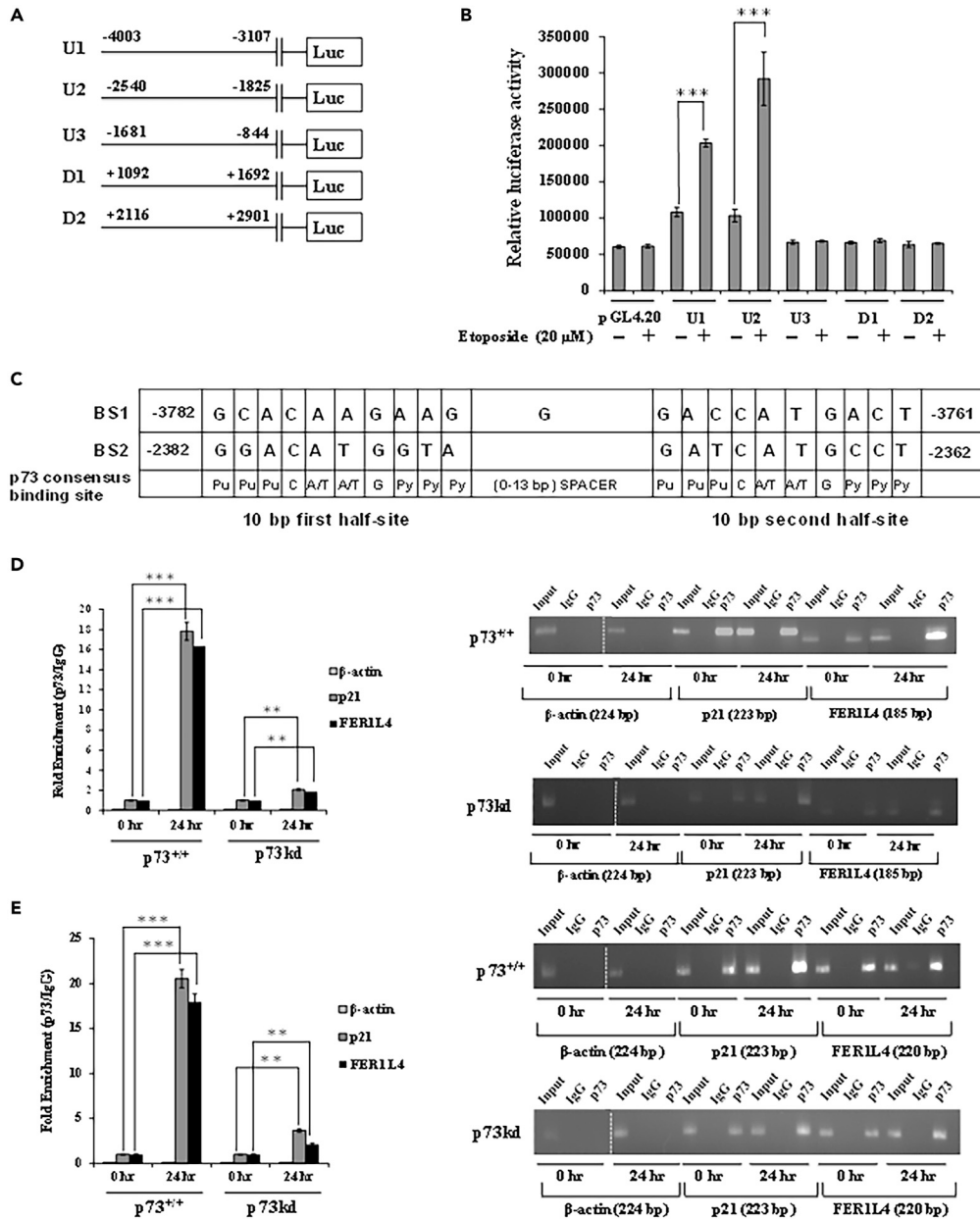
Figure 4. FER1L4 functions as a direct transcriptional target of p73

(A) Schematic portrayal of FER1L4 promoter regions cloned upstream of the luciferase reporter gene in pGL4.20 vector.

(B) Luciferase reporter assay in untreated and etoposide-treated (20 μM, 48 h) HCT116p53$^{-/-}$p73$^{+/+}$ cells transfected with empty pGL4.20 vector or pGL4.20-FER1L4 promoter-reporter constructs and pRL-TK. The results are recorded as mean ± SD of three independent experiments (unpaired two-tailed Student's t test, ***p < 0.001)

(C) Schematic portrayal of two prospective p73-binding sites, BS1 (−3781 to −3761) located in U1 region and BS2 (−2381 to −2362) located in U2 region of FER1L4 promoter

(D and E) ChIP qRT-PCR conducted in etoposide-treated (20 μM) HCT116p53$^{-/-}$p73$^{+/+}$ (Control) and HCT116p53$^{-/-}$p73kd (p73kd) cells for the desired time points with p73 antibody and primers particularly designed for BS1 binding site located in U1 region (D) and BS2 binding site located in U2 region (E) of FER1L4 promoter. β-Actin was kept as a negative control and p21 as a positive control. The results are recorded as mean ± SD of three independent experiments (paired two-tailed Student's t test, **p < 0.01, ***p < 0.001). The three samples (Input, IgG, and p73 pull down) for negative control β-actin (0 h) were run on the same gel but under another 15-well comb so that the size of the combs remained the same. They were merged in the final picture

Figure 5. The exact binding site of p73 was validated by site-directed mutagenesis

(A and B) Schematic portrayal of luciferase reporter plasmids with mutations (boldface) created in BSI in U1 region (A) and BS2 in U2 region (B) of p73-binding site (underlined) in FER1L4 promoter

(C) Luciferase reporter experiment in untreated and etoposide-treated (20 μM) HCT116p53$^{-/-}$p73$^{+/+}$ cells transfected with plasmids having mutations in BS1 and BS2 p73-binding sites. The results are recorded as mean ± SD of three independent experiments (unpaired two-tailed Student's t test, **$p < 0.01$, ***$p < 0.001$).

with the control (Figure 4B). We discovered two complete p73-binding sites BS1 (−3781 to −3761) and BS2 (−2,381 to −2,362) present in the U1 and U2 regions of FER1L4 promoter, respectively (Figure 4C), having least mismatches with the p73 complete binding sequence.

To further attest the direct binding of p73 with FER1L4 promoter *in vivo* and to pinpoint the binding site, chromatin immunoprecipitation (ChIP) assays were conducted. HCT116p53$^{-/-}$p73$^{+/+}$ and p73kd cells were subjected to etoposide (20 μM) treatment for indicated time points, following which ChIP was conducted using p73 antibody. qRT-PCR was performed using the immunoprecipitated DNA and the total input DNA along with primers that flanked the putative p73-binding site BS1; BSS1 (−3,781 to −3,761) located in the U1 region of FER1L4 promoter to give rise to an expected 185-bp product and BS2 site; BSS2 (−2,381 to −2,362) located in the U2 region of FER1L4 promoter, to produce a 220-bp product. B-actin was used as a negative control, and p21 was kept as a positive control. Endogenous p73 was identified to interact specifically with BS1 (Figures 4D and S6A) as well as with BS2 (Figures 4E and S6B), and the fold enrichment amplified with an increase in the duration of etoposide treatment. In contrast, no noteworthy increase in binding to FER1L4 promoter (BS1 and BS2) was detected in etoposide-treated p73kd cells. These results clearly demonstrated that p73 binds the predicted sequences (BS1 and BS2) directly in the FER1L4 promoter to induce FER1L4 transcription *in vivo*.

p73-binding sites in FER1L4 promoter were confirmed by site-directed mutagenesis

To validate the binding of p73 to BS1 and BS2 sites, luciferase reporter constructs having mutations in the core sequence of BS1 (Figure 5A) and BS2 (Figure 5B) p73-binding sites were created by nucleotide substitutions. Luciferase assay was conducted 24 h post etoposide treatment. Mutation of CAAG to AGAT

Figure 6. FER1L4kd enhances the invasion and migration of colorectal cancer cells

(A) Etoposide-treated (20 μM, 24 h) HCT116p53$^{-/-}$p73kd (p73kd) cells were transfected with FER1L4 overexpression plasmid, and quantitative real-time PCR was carried out to quantify FER1L4 mRNA levels in comparison with etoposide-treated HCT116p53$^{-/-}$p73$^{+/+}$ cells (Control) and etoposide-treated HCT116p53$^{-/-}$p73kd cells transfected with empty pCDH plasmid. The results were normalized with β-actin. The results of three independent experiments are recorded as mean ± SD (unpaired two-tailed Student's t test, ***$p < 0.0001$)

(B) Wound healing experiment (B) and its quantification (C) utilizing etoposide-treated (20 μM) HCT116p53$^{-/-}$p73$^{+/+}$ (Control – HCT116p53$^{-/-}$p73$^{+/+}$ cells transfected with scrambled siRNA), si-FER1L4 (FER1L4kd – HCT116p53$^{-/-}$p73$^{+/+}$ cells transfected with siRNA against FER1L4), HCT116p53$^{-/-}$p73$^{+/+}$ (Control – HCT116p53$^{-/-}$p73$^{+/+}$ cells transfected with scrambled shRNA), HCT116p53$^{-/-}$p73kd (p73kd – HCT116p53$^{-/-}$p73$^{+/+}$ cells transfected with specific shRNA against p73), and HCT116p53$^{-/-}$p73kd cells transfected with FER1L4 overexpression plasmid. Images were captured every 12 h to measure the width of the wound using live cell imaging system. The data presented are representative of three

Figure 6. Continued

independent experiments. The results are recorded as mean $\pm$ SD (paired two-tailed Student's t test, $**p < 0.01$, $***p < 0.001$). The migration (D) and invasion (E) capacity of etoposide-treated (20 μM) HCT116p53$^{-/-}$p73$^{+/+}$ (Control – HCT116p53$^{-/-}$p73$^{+/+}$ cells transfected with scrambled siRNA), HCT116p53$^{-/-}$p73kd (p73kd – HCT116p53$^{-/-}$p73$^{+/+}$ cells transfected with specific shRNA against p73), and si-FER1L4 (FER1L4kd – HCT116p53$^{-/-}$p73$^{+/+}$ cells transfected with siRNA against FER1L4) cells by Trevigen's Cultrex 24-well migration assay (D) and Transwell invasion assay (E) after 24 h was also explored. The data presented are representative of three independent experiments. Results are recorded as mean $\pm$ SD (unpaired two-tailed Student's t test, $**p < 0.01$, $***p < 0.001$)

(F) Western blot experiment was conducted with different proteins using cell lysate of etoposide-treated (20 μM, 24 h) HCT116p53$^{-/-}$p73$^{+/+}$ (Control – HCT116p53$^{-/-}$p73$^{+/+}$ cells transfected with scrambled siRNA), si-FER1L4 (FER1L4kd – HCT116p53$^{-/-}$p73$^{+/+}$ cells transfected with siRNA against FER1L4), and HCT116p53$^{-/-}$p73kd (p73kd – HCT116p53$^{-/-}$p73$^{+/+}$ cells transfected with specific shRNA against p73) cells. β-Actin was kept as a loading control. The data presented are representative of three independent experiments

in the first half-site of BS1 binding site (U1 mut1) resulted in a 2.5-fold decrease in the luciferase levels. An equivalent mutation in the second half-site of BS1 binding site (U1 mut2) led to a 2.9-fold depletion in the luciferase levels even in the absence of etoposide. A 5.75-fold decrease in the luciferase levels of U1 mut1 was detected after etoposide treatment, whereas a 5.25-fold decrease was detected in the case of U1 mut2 after etoposide treatment, indicating that both the half-sites are crucial for p73 binding. Mutating both the half-sites (U1 mut1+2) invalidated almost entirely the binding of p73 as negligible luciferase activity was detected (Figure 5C). Likewise, in the absence of etoposide treatment, mutating CATG to AGTT in the first half-site of BS2 binding site (U2 mut1) resulted in no alteration in the luciferase levels. Mutating CATG to AGTT in the second half-site of BS2 binding site (U2 mut2) also led to negligible change in the luciferase levels. In the etoposide-treated cells, mutations in the two half-sites of BS2 gave similar results with 7.5-fold and 7.4-fold decrease in luciferase levels with U2 mut1 and U2 mut2, respectively. Mutating both the half-sites (U2 mut1+2) abrogated practically entire p73 responsiveness (Figure 5C), indicating that both the half-sites of BS2 are equally necessary for p73 binding. These results attest that p73 binds specifically with both BS1 and BS2 binding sites located in FER1L4 promoter to regulate its expression.

FER1L4 knockdown enhances the migration and invasion rate of colorectal cancer cells

We next investigated the function of FER1L4 in p73-mediated inhibition of migration and invasion of colorectal cancer cells. In this direction, we first conducted rescue experiments by transfecting FER1L4 overexpression plasmid in HCT116p53$^{-/-}$p73kd cells, and quantitative real-time PCR indicated that FER1L4 levels increased significantly in p73kd cells after transfection with FER1L4 overexpression plasmid as compared with the control cells transfected with empty plasmid (Figure 6A). To evaluate whether FER1L4 knockdown influences the migration capacity of colorectal cells, wound healing assay was conducted in HCT116p53$^{-/-}$p73$^{+/+}$ (Control – HCT116p53$^{-/-}$p73$^{+/+}$ cells transfected with scrambled siRNA), si-FER1L4 (FER1L4kd – HCT116p53$^{-/-}$p73$^{+/+}$ cells transfected with siRNA against FER1L4), HCT116p53$^{-/-}$p73$^{+/+}$ (Control – HCT116p53$^{-/-}$p73$^{+/+}$ cells transfected with scrambled shRNA), and p73kd (HCT116p53$^{-/-}$p73$^{+/+}$ cells transfected with shRNA against p73) cells. Cells were seeded and subjected to etoposide (20 μM) treatment after 24 h. After this, a wound was fashioned and images were captured after every 12 h. Under genotoxic stress produced by etoposide, the migration of FER1L4kd cells and p73kd cells was significantly enhanced as compared with that of the control cells (Figures 6B and 6C). Furthermore, when p73kd cells were transfected with FER1L4 overexpression plasmid, cell migration reduced significantly as compared with FER1L4kd and p73kd cells, further indicating that re-expression of FER1L4 is sufficient to reinstate the suppression of the migratory phenotype of the cells (Figures 6B and 6C). To further corroborate our findings, we assessed the migration capacity of FER1L4kd and p73kd cells through Trevigen's Cultrex 24-well migration assay. Cells were seeded and subjected to etoposide (20 μM) treatment for 24 h. In line with the previous observations, FER1L4kd and p73kd cells portrayed a significantly greater percentage of migration compared with that of the control cells (Figure 6D). Following this, we assessed the invasive capacity of HCT116p53$^{-/-}$p73$^{+/+}$ (Control), FER1L4kd, and p73kd cells through Trevigen's Cultrex 24-well invasion assay. Cells were seeded and subjected to etoposide (20 μM) treatment for 24 h. Cells were permitted to invade according to their invasive capacity through membrane pores to the lower chamber for 24 h after etoposide treatment. The FER1L4kd cells demonstrated almost 40% enhanced invasive ability as compared with the control cells. Similarly, p73kd cells portrayed an identical trend as that of FER1L4kd cells (Figure 6E). Collectively, these results portray that FER1L4 regulates cell invasion and migration in a p73-regulated manner. Simply put, these results firmly indicate that p73 employs its anti-migratory and anti-invasion ability by enhancing lncRNA FER1L4 expression.
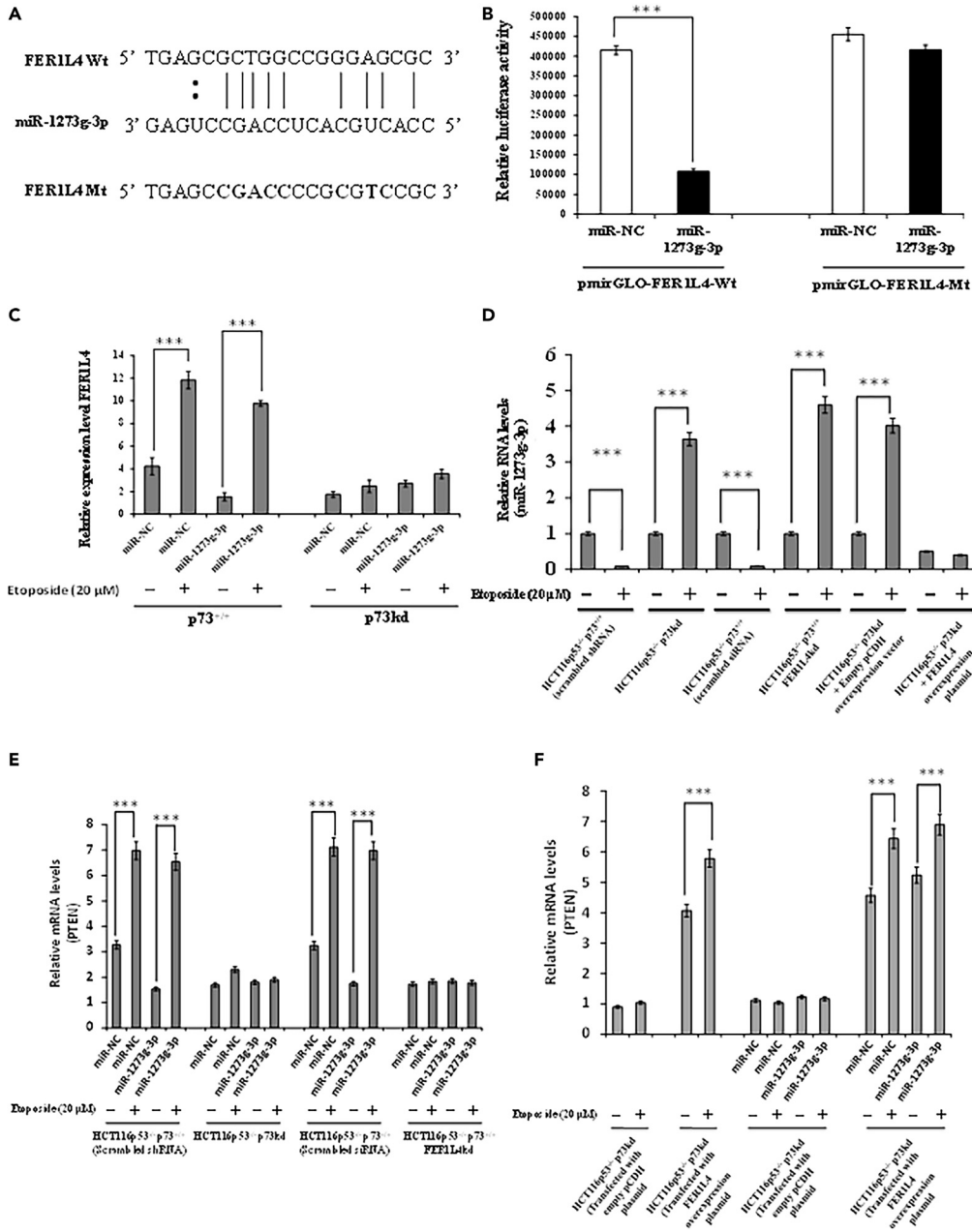
Figure 7. FER1L4 interacts with miR-1273g-3p

(A) The predicted miR-1273g-3p-binding site in FER1L4 3′ UTR region and its corresponding mutated sequences

(B) Dual luciferase reporter plasmid carrying wild-type or mutant FER1L4 3′ UTR region (FER1L4-Wt or FER1L4-Mt) was co-transfected with miR-NC and miR-1273g-3p. The data are recorded as mean ± SD from three independent experiments (unpaired two-tailed Student's t test, ***p < 0.001)

(C) The expression levels of FER1L4 in untreated and etoposide-treated (20 μM, 24 h) HCT116p53$^{-/-}$p73$^{+/+}$ (Control) and HCT116p53$^{-/-}$p73kd (p73kd) cells transfected with miR-NC and miR-1273g-3p was analyzed by RT-qPCR, normalized with β-actin. The data are recorded as mean ± SD from three independent experiments (unpaired two-tailed Student's t test, ***p < 0.001)

(D) The expression of miR-1273g-3p in untreated and etoposide-treated (20 μM, 24 h) HCT116p53$^{-/-}$p73$^{+/+}$ (Control – HCT116p53$^{-/-}$p73$^{+/+}$ cells transfected with scrambled shRNA), HCT116p53$^{-/-}$p73kd (p73kd – HCT116p53$^{-/-}$p73$^{+/+}$ cells transfected with specific shRNA targeting p73), HCT116p53$^{-/-}$p73$^{+/+}$ (Control – HCT116p53$^{-/-}$p73$^{+/+}$ cells transfected with scrambled siRNA), HCT116p53$^{-/-}$p73$^{+/+}$FER1L4kd (FER1L4kd – HCT116p53$^{-/-}$p73$^{+/+}$ cells transfected with specific siRNA against FER1L4), HCT116p53$^{-/-}$p73kd cells transfected with empty pCDH overexpression vector and

Figure 7. Continued

HCT116p53$^{-/-}$p73kd cells transfected with FER1L4 overexpression vector was analyzed by TaqMan RT-qPCR, normalized with RNU6B endogenous control. The data are recorded as mean ± SD from three independent experiments (unpaired two-tailed Student's *t* test, ***p < 0.001)

(E) The expression of PTEN in untreated and etoposide-treated (20 μM, 24 h) HCT116p53$^{-/-}$p73$^{+/+}$ (Control – HCT116p53$^{-/-}$p73$^{+/+}$ cells transfected with scrambled shRNA), HCT116p53$^{-/-}$p73kd (p73kd – HCT116p53$^{-/-}$p73$^{+/+}$ cells transfected with specific shRNA against p73), HCT116p53$^{-/-}$p73$^{+/+}$ (Control – HCT116p53$^{-/-}$p73$^{+/+}$ cells transfected with scrambled siRNA), and HCT116p53$^{-/-}$p73$^{+/+}$FER1L4kd (FER1L4kd – HCT116p53$^{-/-}$p73$^{+/+}$ cells transfected with specific siRNA against FER1L4) cells transfected with miR-NC and miR-1273g-3p was analyzed by RT-qPCR, normalized with β-actin. The data are recorded as mean ± SD from three independent experiments (unpaired two-tailed Student's *t* test, ***p < 0.001)

(F) The expression of PTEN in untreated and etoposide-treated (20 μM, 24 h) HCT116p53$^{-/-}$p73kd cells transfected with empty pCDH overexpression plasmid and HCT116p53$^{-/-}$p73kd cells transfected with FER1L4 overexpression plasmid transfected with miR-NC and miR-1273g-3p was analyzed by RT-qPCR, normalized with β-actin. The data are recorded as mean ± SD from three independent experiments (unpaired two-tailed Student's *t* test, ***p < 0.001)

Knockdown of FER1L4 advances Epithelial to Mesenchymal Transition (EMT)

Next, we assessed whether FER1L4kd has any effect on the expression of biomarkers involved in invasion and migration, including EMT transition markers such as E-cadherin, N-cadherin, snail, fibronectin, and vimentin. In this direction, HCT116p53$^{-/-}$p73$^{+/+}$ (Control – HCT116p53$^{-/-}$p73$^{+/+}$ cells transfected with scrambled siRNA), si-FER1L4 (FER1L4kd – HCT116p53$^{-/-}$p73$^{+/+}$ cells transfected with siRNA against FER1L4), HCT116p53$^{-/-}$p73$^{+/+}$ (Control – HCT116p53$^{-/-}$p73$^{+/+}$ cells transfected with scrambled shRNA), and p73kd (HCT116p53$^{-/-}$p73$^{+/+}$ cells transfected with shRNA against p73) cells were given etoposide (20 μM) treatment for 24 h and western blotting was conducted. Results portrayed that FER1L4 knockdown cells exhibited noteworthy down-regulated protein expression levels of epithelial marker E-cadherin, whereas the expression of the mesenchymal markers, such as Snail, Vimentin, N-cadherin, and Fibronectin, was remarkably up-regulated in FER1L4kd cells as compared with the control cells. In a similar way, p73 knockdown cells also exhibited reduced E-cadherin expression and enhanced N-cadherin, Snail, Vimentin, and Fibronectin expression (Figures 6F, and S7). Collectively, these results corroborate the observation that FER1L4 limits the migration and invasion ability of colorectal cancer cells and plays a key part in inhibition of EMT in a p73-dependent manner.

FER1L4 functions as a competing endogenous RNA and sponges miR-1273g-3p in colorectal cancer

In recent times lncRNAs have been implicated to be engaged in several molecular pathways, for instance, RNA splicing, DNA replication, and regulation of gene expression. Additionally, role of lncRNAs as competing endogenous RNA (ceRNA) has emerged as a new pathway (Fatima et al., 2015; Zhang et al., 2016). It is known that FER1L4 acts as a ceRNA in gastric cancer (Xia et al., 2015), yet lncRNAs function as a ceRNA could sponge multiple miRNAs to modulate several targets. Hence, two target prediction tools RegRNA2.0 and lncRNASNP2 were utilized to assess potential miRNAs that could have prospective binding sites for FER1L4. Bioinformatic results indicated seven miRNAs with potential binding sites for FER1L4 (Figures S8A–S8G). To further screen which miRNA actually binds at the 3′UTR of FER1L4 *in vitro*, reporter plasmids carrying the predicted miRNA wild-type or mutant binding sites (pmirGLO-FER1L4-Wt or pmirGLO-FER1L4-Mt) were generated. These reporter plasmids were co-transfected with the individual miRNA mimics or negative control miRNA (miR-NC) mimic and dual luciferase reporter assay was carried out (Figure S8H). Among the target miRNAs, miR-1273g-3p was chosen for our study, based on the decreased luciferase activity observed by miR-1273g-3p in the presence of pmirGLO-FER1L4-WT compared with the control (cells transfected with miR-NC), whereas pmirGLO-FER1L4-Mt was unable to produce this suppression (Figures S8H, 7A and 7B). A complementary binding site is present in the 3′ UTR region of FER1L4 and miR-1273g-3p (Figure 7A). These results demonstrated that miR-1273g-3p directly binds to FER1L4-binding sites, resulting in down-regulation of the luciferase activity. Transfection of p73$^{+/+}$ cells with miR-1273g-3p under stressed conditions failed to inhibit the etoposide-induced overexpression of FER1L4 (Figure 7C), suggesting that miR-1273g-3p is working downstream of FER1L4.

We therefore conducted experiments to explore the effect of p73 and FER1L4 expression on the levels of miR-1273g-3p. Untreated and etoposide-treated (20 μM, 24 h) HCT116p53$^{-/-}$p73$^{+/+}$, HCT116p53$^{-/-}$p73kd, and HCT116p53$^{-/-}$p73$^{+/+}$FER1L4kd cells were checked for the levels of miR-1273g-3p by quantitative real-time PCR (Figure 7D) using a TaqMan probe designed specifically to target miR-1273g-3p. We observed miR-1273g-3p levels to be significantly decreased in etoposide-treated

HCT116p53$^{-/-}$p73$^{+/+}$ cells as compared with the untreated HCT116p53$^{-/-}$p73$^{+/+}$ cells, whereas in p73kd and FER1L4kd cells, miR-1273g-3p levels were significantly up-regulated as compared with the cells expressing p73 and FER1L4 (Figures 7D, and S9A). Furthermore, we conducted rescue experiments for FER1L4 in p73kd cells and observed that, when transfected with FER1L4 overexpression plasmid, miR-1273g-3p levels decreased significantly as compared with control p73kd cells transfected with empty pCDH overexpression plasmid. These observations lead us to conclude that, when FER1L4 levels are up-regulated in etoposide-treated HCT116p53$^{-/-}$p73$^{+/+}$ cells, it decreases the levels of miR-1273g-3p in cells. On the other hand, when FER1L4 levels decrease in p73kd and FER1L4kd cells, it is unable to sponge the miR-1273g-3p, resulting in its increased levels. To further confirm the direct interaction of FER1L4 and miR-1273g-3p, RNA immunoprecipitation (RIP) experiments were employed in HCT116p53$^{-/-}$p73$^{+/+}$ cell extracts using p73 antibody. As shown in Figure S9B, both lncRNA FER1L4 and miR-1273g-3p were specifically enriched in p73 pull down samples, but not in the control IgG, suggesting that miR-1273g-3p is a bona fide lncRNA-FER1L4-targeting miRNA.

PTEN, an accomplished tumor suppressor, is a known downstream target of miR-1273g-3p that has been shown to suppress PTEN (Niu et al., 2016). To explore the relationship among FER1L4, miR-1273g-3p, and PTEN, HCT116p53$^{-/-}$p73$^{+/+}$ (Control – HCT116p53$^{-/-}$p73$^{+/+}$ cells transfected with scrambled shRNA), p73kd (HCT116p53$^{-/-}$p73$^{+/+}$ cells transfected with shRNA against p73), HCT116p53$^{-/-}$p73$^{+/+}$ (Control – HCT116p53$^{-/-}$p73$^{+/+}$ cells transfected with scrambled siRNA), and si-FER1L4 (FER1L4kd – HCT116p53$^{-/-}$p73$^{+/+}$ cells transfected with siRNA against FER1L4) cells were transfected with miR-NC mimic and miR-1273g-3p mimic in unstressed and stressed conditions using etoposide as genotoxic stress inducer. PTEN expression was significantly up-regulated at mRNA levels in etoposide-treated HCT116p53$^{-/-}$p73$^{+/+}$ cells transfected with miR-NC as compared with that of unstressed cells. Similarly, miR-1273g-3p was unable to decrease the levels of PTEN in HCT116p53$^{-/-}$p73$^{+/+}$ cells in the presence of etoposide as under these conditions the levels of FER1L4 are high (Figure 7E). However, decreased levels of PTEN were observed in both p73kd and FER1L4kd cells. These observations are in agreement with our previous results wherein we observed an increase in the levels of miR-1273g-3p in p73kd and FER1L4kd cells (Figure 7D). We envisage that inhibition of the expression of miR-1273g-3p in HCT116p53$^{-/-}$p73$^{+/+}$ cells would have increased PTEN expression. We also performed FER1L4 rescue experiments in p73kd cells and observed that, when transfected with FER1L4 overexpression plasmid, PTEN levels increased significantly in the presence or absence of genotoxic stress as compared with the control cells transfected with empty pCDH overexpression plasmid (Figure 7F). We further observed that, upon co-transfection with miR-1273g-3p mimics, PTEN levels still increased significantly as FER1L4 overexpression sponged the levels of miR-1273g-3p (Figure 7F). We also evaluated PTEN protein expression levels in untreated and etoposide-treated (20 μM, 24 h) HCT116p53$^{-/-}$p73$^{+/+}$ (Control – HCT116p53$^{-/-}$p73$^{+/+}$ cells transfected with scrambled shRNA), p73kd (HCT116p53$^{-/-}$p73$^{+/+}$ cells transfected with shRNA against p73), HCT116p53$^{-/-}$p73$^{+/+}$ (Control – HCT116p53$^{-/-}$p73$^{+/+}$ cells transfected with scrambled siRNA), si-FER1L4 (FER1L4kd – HCT116p53$^{-/-}$p73$^{+/+}$ cells transfected with siRNA against FER1L4), and HCTT16p53$^{-/-}$p73kd cells transfected with FER1L4 overexpression plasmid, in the presence and absence of miR-NC and miR-1273g-3p. In line with the qPCR results, PTEN protein levels were also increased in the presence of genotoxic stress in control cells. However, in p73kd and FER1L4kd cells, PTEN levels decreased. Upon overexpression of FER1L4 in p73kd cells, PTEN levels increased even in the presence of miR-1273g-3p, indicating that enhanced levels of FER1L4 sponge the action of miR-1273g-3p, leading to enhanced expression of PTEN (Figure S9C). Taken together, our results clearly indicate that FER1L4 functions upstream of miR-1273g-3p and inhibits its oncogenic potential, leading to an increase in PTEN levels, which further causes cell-cycle arrest.

RNA *in situ* hybridization investigation of FER1L4 and p73 mRNA expression levels in non-metastatic and metastatic colon cancer tissues

To attest the positive correlation between FER1L4 and p73, 15 samples each of human non-metastatic and metastatic colorectal cancer (CRC) tissues were assessed for FER1L4 and p73 mRNA expression by RNA-ISH (Table S1). The p73 protein is located mainly in the nuclei of the cancer cells, whereas FER1L4 is expressed mainly in the cytoplasm of the cancer cells. The p73 expression level was remarkably higher in non-metastatic CRC tissue samples as compared with metastatic colon cancer tissue samples (Figure 8A—compare a and c, b and d; Figure S10A). Similarly, FER1L4 expression was significantly enhanced in non-metastatic CRC tissue samples as compared with metastatic CRC tissue samples (Figure 8B—compare a and b, c and d; Figure S10B). Association studies were also carried out to ascertain the correlation between p73 and FER1L4 expression in non-metastatic and metastatic tissue samples, respectively (Figures 8C and 8D). We conducted scoring of the expression pattern on a scale of 1–4 based on the intensity of staining. 1All of 15 cases of non-metastatic CRC portrayed enhanced intensity (2 or 3)
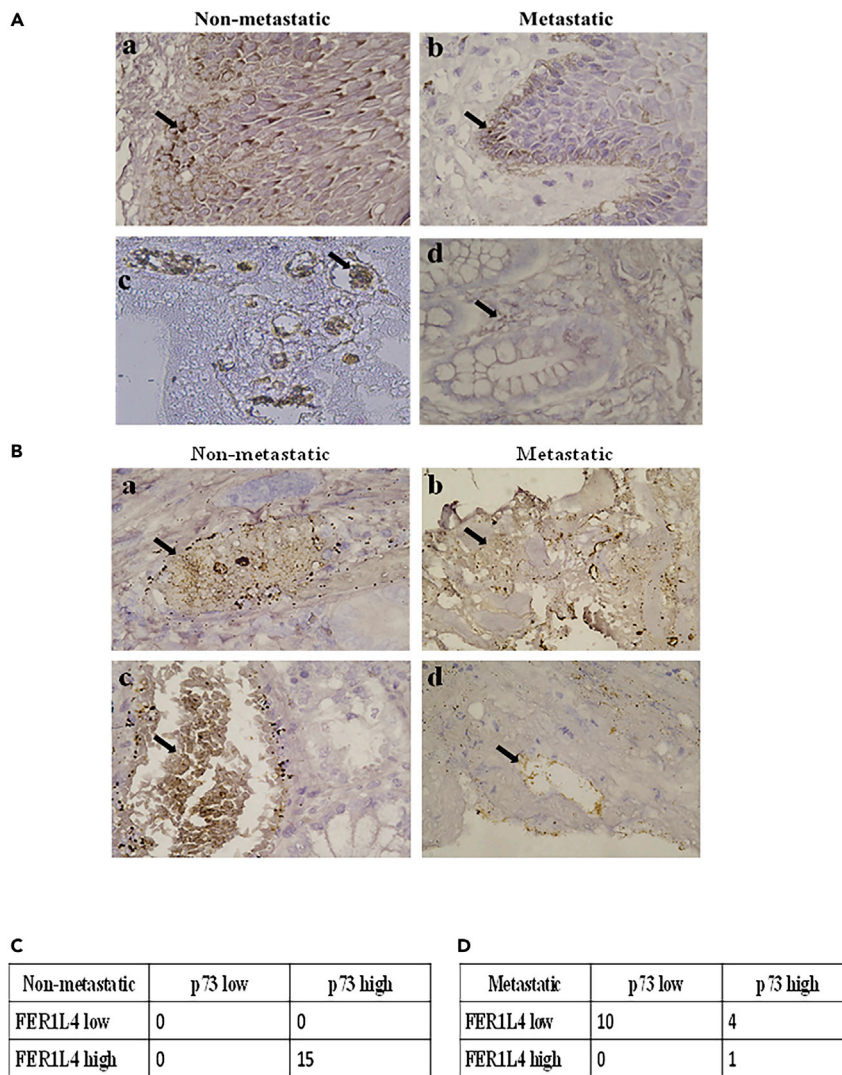
Figure 8. Differential expression of FER1L4 and p73 mRNA in metastatic and non-metastatic colon cancer tissue samples

(A) Fifteen samples of human non-metastatic and fifteen samples of human metastatic colorectal cancer tissues were evaluated for FER1L4 and p73 mRNA expression by RNA *in situ* hybridization (RNA-ISH)

(A and B) Representative images of RNA-ISH for p73 (A) and FER1L4 (B) mRNA expression in non-metastatic and metastatic colon carcinoma tissue samples (magnification X600). The arrows in A (a, b, c, and d) represent p73 expression observed mainly in the nuclei of the cancer cells. The arrows in B (a, b, c, and d) represent FER1L4 expression observed mainly in the cytoplasm of the cancer cells

(C) Association study between p73 and FER1L4 expression in non-metastatic CRC tissue samples

(D) Association study between p73 and FER1L4 expression in metastatic CRC tissue samples

for both FER1L4 and p73 expression. On the other hand, 9/15 cases of metastatic CRC portrayed decreased intensity (0 or 1) for both FER1L4 and p73 expression. Based on our results of p73kd and FER1L4kd cell lines and RNA-ISH, we anticipate that this significant down-regulation of p73 and FER1L4 mRNA levels could augment metastasis in colon cancer.

DISCUSSION

Over the past few years, research on the role of microRNAs in regulating malignant diseases has governed the field of non-coding RNA regulation (Borel et al., 2012), but the consequences of lncRNA in the tumorigenesis of colon cancer are still unknown to a large extent. Accumulating evidences suggest that a

plethora of lncRNAs could be utilized as diagnostic biomarkers and therapeutic targets in human cancers and portray oncogenic or tumor suppressor functions in human cancer pathogenesis. For example, colon cancer-associated transcript-2 (CCAT-2) expression is enhanced in breast cancer and reduction of CCAT2 expression inhibits cell proliferation and invasion of both MCF7 and MDA-MB 231 breast cancer cells (Cai et al., 2015). The tumor-suppressive role of lncRNA DREH (Down-regulated expression by HBx) is regulated by alterations in the architecture of the cytoskeleton as a result of binding to vimentin and inhibition of vimentin expression. Knockdown of DREH in hepatocellular carcinoma (HCC) cells through RNAi enhances migration and invasion (Huang et al., 2013). The expression of Homeobox transcript antisense intergenic RNA (HOTAIR) corresponds with metastasis and bad prognosis in breast, colon, and lung cancer (Chrisholm et al., 2012; Kogo et al., 2011; Loewen et al., 2014). LncRNA LET (Low expression in tumor) expression is decreased in HCC and corresponds with metastasis (Yang et al., 2011, 2013). Its mechanism of action depends on binding to NF90, a double-stranded RNA-binding protein, causing ubiquitinylation and degradation of NF90. All these findings indicate that lncRNAs function as regulators and influence various biological circuits and portray a pivotal regulatory role in carcinogenesis. Hence, identification of novel lncRNAs and understanding the prospective molecular pathways would enhance the advancement of lncRNA-directed diagnostics and therapies against cancers.

LncRNA FER1L4 has been disclosed to be engaged in initiation and development of several cancers by modulating cancer cell proliferation, apoptosis, and metastasis (;; Ding et al., 2017; Fatima et al., 2015; Liu et al., 2014; Qiao and Li, 2016; Wu et al., 2017; Xia et al., 2015; Yue et al., 2015). It was initially identified as existing in gastric cancer and is down-regulated in gastric cancer tissues as compared with surrounding normal tissues (Song et al., 2013). Wu et al. (2017) demonstrated that FER1L4 exerts a tumor inhibitory action on liver cancer by suppression of miR-106a-5p expression. Qiao and Li (2016) demonstrated that FER1L4 subdues cancer cell proliferation by modulating PTEN levels in endometrial carcinoma. A recent study also proposed that FER1L4 induces osteogenic differentiation of human periodontal ligament stromal cells through miR-874-3p and vascular endothelial growth factor A (Huang et al., 2020). However, the regulation and underlying mechanism of tumor-suppressive role of FER1L4 in colorectal cancer was unexplored.

In our study, we attested for the first time the association of FER1L4 and p73 tumor suppressor gene with colon cancer progression. As a tumor suppressor, p73 modulates several crucial cellular pathways, including cell cycle progression, apoptosis, genomic stability, metabolism, and metastasis (Allocati et al., 2012; Napoli and Flores, 2017; Nicolai et al., 2015; Ozaki et al., 2010; Satija and Das, 2016; Yoon et al., 2015). Our laboratory also recently identified that p73 exerts its anti-metastatic role through up-regulation of Navigator-3, a microtubule binding protein, and inhibits the migration, invasion, and metastasis of colorectal cancer cells (Uboveja et al., 2020). But still the mechanism of p73 in CRC metastasis is unclear and needs to be dissected further. In line with this direction, our study bestows conclusive proof that p73 transcriptionally regulates long non-coding RNA FER1L4 and exerts its tumor-suppressive effects through up-regulation of FER1L4 under genotoxic stress.

Our study reveals the molecular mechanisms aiding the crucial function of p73 in restriction of metastasis by regulation of FER1L4. Identification of two prospective p73-binding sites in the FER1L4 promoter region instigated us to investigate whether p73 modulates FER1L4 expression. HCT116p53$^{-/-}$p73$^{+/+}$ cells subjected to etoposide activated endogenous p73, with an associated enhancement in the mRNA levels of FER1L4. In addition, luciferase reporter experiments demonstrated that the prospective p73-binding sites in FER1L4 promoter are functional and initiate transcription in a p73-regulated manner. Essentially, other constructs that either did not possess p73-binding sites or carried mutations within the prospective site demonstrated no p73-dependent transcriptional activation of reporter gene, indicating that the predicted p73-binding sites are actually required for p73-mediated transcriptional activation of FER1L4. The association of p73 with FER1L4 promoter under *in vivo* conditions was indisputably confirmed by ChIP experiments.

The functional importance of FER1L4 regulation by p73 was ascertained by conducting wound healing experiments and Transwell migration and invasion assays. These assays revealed that FER1L4 knockdown increased colon cancer cell migration and invasion in a p73-dependent way. Essentially, FER1L4 functions downstream of p73 and specifically regulates cell migration as in p73kd cells, the migration rates were similar to that of FER1L4kd cells. EMT is a phenotypic change in which epithelial cells lose their polarity and cell adhesion property and undergo various biochemical alterations, becoming motile non-polarized

mesenchymal cells with migratory and invasive properties (Boyer et al., 2000; Vu and Datta, 2017). A broadly trusted marker for EMT is the loss of E-cadherin (Vleminckx et al., 1991) and up-regulation of N-cadherin (Hazan et al., 2000), Vimentin (Hendrix et al., 1997), Snail (Batlle et al., 2000), and Fibronectin (Park and Schwarzbauer, 2014). FER1L4kd and p73kd cells demonstrated a significant decrease in the expression of E-cadherin, and noteworthy up-regulation of the mesenchymal markers as compared with that of the control cells, thereby indicating that FER1L4 plays a significant role as a metastasis deterrent in a p73-dependent manner. Collectively, these results firmly indicate that p73 exerts its anti-metastatic activity through up-regulation of lncRNA FER1L4.

LncRNAs carry out regulatory activities in cancers through a sophisticated circuit, the ceRNA regulatory circuit by which lncRNAs can sponge miRNAs and then liberate the miRNA target gene to augment either tumor progression or suppression. Furthermore, reports have ascertained that FER1L4 acts as a ceRNA to exert its regulatory function in multiple cancers. For instance, FER1L4 acts as a ceRNA to modulate PTEN expression by functioning as a sponge for miR-106a-5p in gastric cancer (Xia et al., 2015). Another study has reported that FER1L4, functioning as a ceRNA for miR-18a-5p, carries out its anti-cancer function by regulating the expression of PTEN in osteosarcoma (Fei et al., 2018). FER1L4 has also been found to suppress oncogenesis by interacting with miR-106a-5p in colon cancer (Yue et al., 2015). Furthermore, as a ceRNA, FER1L4 can sponge multiple miRNAs to carry out its regulatory activity. Hence, we screened bioinformatics databases and identified seven miRNAs that could possess FER1L4-binding sites. Based on literature review, miR-1273g-3p was chosen as a potential candidate that FER1L4 can interact with. miR-1273g-3p has an oncogenic role, which has been confirmed in many studies. For instance, it has been validated that miR-1273g-3p augments proliferation, migration, and invasion of colorectal cancer cells by inducing ERBB4/PIK3R3/mTOR/S6K2 signaling mechanism (Li et al., 2018). To understand the relationship between FER1L4 and miRNA-1273g-3p we carried out series of experiments, viz., (1) a dual luciferase assay, which demonstrated that, in the presence of miR-1273g-3p, the luciferase levels dropped with constructs carrying FER1L4wt region compared with that of cells transfected with constructs carrying mutated FER1L4 (FER1L4-Mt) region in the presence of miR-1273g-3p; (2) under genotoxic stress, transfection with miR-1273g-3p failed to down-regulate the levels of FER1L4; (3) both the p73kd and FER1L4kd cells showed high levels of miR-1273g-3p under genotoxic stress, whereas in p73$^{+/+}$ cells, levels of miR-1273g-3p were low; and (4) when p73kd cells are transfected with FER1L4 overexpression plasmid, it leads to a significant decrease in miR-1273g-3p levels even when transfected with miR-1273g-3p mimics as FER1L4 is able to sponge the expression of miR-1273g-3p. Taken together, all these experiments strongly suggest that FER1L4 regulates the levels of miR-1273g-3p and not vice versa. To further support our observations, we investigated the expression of PTEN, a known downstream target of miR-1273g-3p, in p73$^{+/+}$, p73kd, and FER1L4kd cells. We found that PTEN expression was significantly increased in etoposide-treated p73$^{+/+}$ cells, whereas low levels of PTEN were observed in p73kd and FER1L4kd cells. Furthermore, there was a significant increase in PTEN expression levels in p73kd cells transfected with FER1L4 overexpression plasmid even in the presence of miR-1273g-3p mimics. We conclude that increased levels of FER1L4 in p73$^{+/+}$ cells sponge miR-1273g-3p and thereby inhibit its oncogenic functions, whereas low levels of FER1L4 in FER1L4kd cells will result in high levels of miR-1273g-3p, leading to the increased proliferation rates and decreased apoptosis.

Our previous study assessed p73 expression in tumor tissues of patients with CRC and identified reduced p73 expression in CRC tumor tissue as compared with normal colon tissue (Kotulak et al., 2016; Uboveja et al., 2020). In this direction, we compared the mRNA expression of FER1L4 and p73 by RNA-ISH in metastatic and non-metastatic colon cancer tissues and determined whether there exists co-expression of FER1L4 and p73 as suggested in our study. Notably, we detected reduced mRNA expression of both FER1L4 and p73 in metastatic tissues as compared with non-metastatic tissues, further confirming our observations. Additionally, a significant association between FER1L4 and p73 mRNA levels was observed in both non-metastatic and metastatic tissue samples. These findings suggest that FER1L4 expression is positively governed by p73 overexpression in colorectal cancers to restrict cancer cell metastasis, whereas inhibition of p73 results in decreased FER1L4 expression in colorectal cancer cells, leading to enhanced metastatic activity of cancer cells.

Collectively, our study gives conclusive proof that p73 acts as a positive transcriptional modulator that directly regulates lncRNA FER1L4 and FER1L4 is crucial for p73-mediated suppression of colorectal cancer cell invasion, migration, and metastasis.

Limitations of the study

Our *in vitro* data reveal that, upon genotoxic stress, p73 tumor suppressor gene gets upregulated and increases the levels of FER1L4 lncRNA. The positive correlation between p73 and FER1L4 lncRNA has been established by various experiments in p53$^{-/-}$ colorectal cancer cell line and by RNA-ISH experiment in metastatic and non-metastatic colorectal cancer tissue samples. Later on, we further prove that FER1L4 lncRNA sponges the oncogenic potential of miRNA-1273g-3p by various experiments in p53$^{-/-}$ colorectal cancer cell line. However, this negative correlation between FER1L4 lncRNA and miR-1273g-3p should have been further confirmed in colorectal cancer patient samples, which could not be completed and included in this article.

DATA AVAILABILITY STATEMENT

The data that support the findings of this study are available on request from the corresponding author. The data are not publicly available owing to privacy or ethical restrictions.

STAR★METHODS

Detailed methods are provided in the online version of this paper and include the following:

- KEY RESOURCES TABLE
- RESOURCE AVAILABILITY
  - Lead contact
  - Materials availability
  - Data and code availability
- EXPERIMENTAL MODEL AND SUBJECT DETAILS
  - Tissue samples
  - Cell lines
- METHOD DETAILS
  - Plasmids and shRNA
  - Luciferase assays
  - Cell counting kit 8 (CCK-8) assay
  - Ethynyldeoxyuridine (EdU) assay
  - Cell cycle analysis
  - QuantiGene ViewRNA ISH cell assay
  - Terminal deoxynucleotidyltransferase dUTP nick end labelling (TUNEL) assay
  - Chromatin immunoprecipitation (ChIP) assays
  - RNA immunoprecipitation assay
  - Site-directed mutagenesis assay
  - Annexin-V/propidium iodide assay
  - Western blotting analysis
  - Migration assay measured using calcein-AM
  - Invasion assay measured using Calcein-AM
  - Wound-healing assay
  - RNA extraction and qRT-PCR
  - RNA-*In situ* hybridization (RNA-ISH)
- QUANTIFICATION AND STATISTICAL ANALYSIS
  - Statistics

SUPPLEMENTAL INFORMATION

Supplemental information can be found online at https://doi.org/10.1016/j.isci.2022.103811.

for Bioinformatics Facility (DBT-BIF) at Dr. B.R. Ambedkar Center for Biomedical Research is highly acknowledged. Junior and Senior Research Fellowship to A.U. from DBT (DBT/JRF/15/AL/36) is gratefully acknowledged.

AUTHOR CONTRIBUTIONS

DECLARATION OF INTERESTS

REFERENCES

Allocati, N., Di Ilio, C., and De Laurenzi, V. (2012). p63/p73 in the control of cell cycle and cell death. Exp. Cell Res. *318*, 1285–1290.

Batista, P.J., and Chang, H.Y. (2013). Long noncoding RNAs: cellular address codes in development and disease. Cell *152*, 1290–1298.

Batlle, E., Sancho, E., Francí, C., Domínguez, D., Monfar, M., Baulida, J., and García De Herreros, A. (2000). The transcription factor snail is a repressor of E-cadherin gene expression in epithelial tumour cells. Nat. Cell Biol. *2*, 84–89.

Borel, F., Konstantinova, P., and Jansen, P.L. (2012). Diagnostic and therapeutic potential of miRNA signatures in patients with hepatocellular carcinoma. J. Hepatol. *56*, 1371–1383.

Boyer, B., Vallés, A.M., and Edme, N. (2000). Induction and regulation of epithelial-mesenchymal transitions. Biochem. Pharmacol. *60*, 1091–1099.

Cai, Y., He, J., and Zhang, D. (2015). Long noncoding RNA CCAT2 promotes breast tumor growth by regulating the Wnt signaling pathway. OncoTargets Ther. *8*, 1099–2657. https://doi.org/10.2147/OTT.S90485.

Chen, S., Li, P., Xiao, B., and Guo, J. (2014). Long noncoding RNA HMlincRNA717 and AC130710 have been officially named as gastric cancer associated transcript 2 (GACAT2) and GACAT3, respectively. Tumour Biol. *35*, 8351–8352.

Chrisholm, K.M., Wan, Y., Li, R., Montgomery, K.D., Chang, H.Y., and West, R.B. (2012). Detection of long non-coding RNA in archival tissue: correlation with polycomb protein expression in primary and metastatic breast carcinoma. PLoS One *7*, e47998.

Ding, F., Tang, H., Nie, D., and Xia, L. (2017). Long non-coding RNA Fer-1-like family member 4 is overexpressed in human glioblastoma and

regulates the tumorigenicity of glioma cells. Oncol. Lett. *14*, 2379–2384.

Dötsch, V., Bernassola, F., Coutandin, D., Candi, E., and Melino, G. (2010). p63 and p73, the ancestors of p53. Cold Spring Harb. Perspect. Biol. *2*, a004887.

Fatima, R., Akhade, V.S., Pal, D., and Rao, S.M. (2015). Long noncoding RNAs in development and cancer: potential biomarkers and therapeutic targets. Mol. Cell Ther. *3*, 5.

Fei, D., Zhang, X., Liu, J., Tan, L., Xing, J., and Zhao, D. (2018). Long noncoding RNA FER1L4 suppresses tumorignesis by regulating the expression of PTEN targeting miR-18a-5p in osteosarcoma. Cell Physiol. Biochem. *51*, 1363–1375.

Fernandes, J.C.R., Acuña, S.M., Aoki, J.I., Floeter-Winter, L.M., and Muxel, S.M. (2019). Long non-coding RNAs in the regulation of gene expression: physiology and disease. Noncoding RNA *5*, 17.

Gao, Q., and Zheng, J. (2018). microRNA-323 upregulation promotes prostate cancer growth and docetaxel resistance by repressing p73. Biomed. Pharmacother. *97*, 528–534.

Geisler, S., and Coller, J. (2013). RNA in unexpected places: long non-coding RNA functions in diverse cellular contexts. Nat. Rev. Mol. Cell Biol. *14*, 699–712.

Hazan, R.B., Phillips, G.R., Qiao, R.F., Norton, L., and Aaronson, S.A. (2000). Exogenous expression of N-cadherin in breast cancer cells induces cell migration, invasion, and metastasis. J. Cell Biol. *148*, 779–790.

Hendrix, M.J., Seftor, E.A., Seftor, R.E., and Trevor, K.T. (1997). Experimental co-expression of vimentin and keratin intermediate filaments in human breast cancer cells results in phenotypic

interconversion and increased invasive behavior. Am. J. Pathol. *150*, 483–495.

Huang, J.F., Guo, Y.J., Zhao, C.X., Yuan, S.X., Wang, Y., Tang, G.N., Zhou, W.P., and Sun, S.H. (2013). Hepatitis B virus X protein (HBx)-related long noncoding RNA (lncRNA) down-regulated expression by HBx (Dreh) inhibits hepatocellular carcinoma metastasis by targeting the intermediate filament protein vimentin. Hepatology *57*, 1882–1892.

Huang, Y., Han, Y., Guo, R., Liu, H., Li, X., Jia, L., Zheng, Y., and Li, W. (2020). Long non-coding RNA FER1L4 promotes osteogenic differentiation of human periodontal ligament stromal cells via miR-874-3p and vascular endothelial growth factor A. Stem Cell Res. Ther. *11*, 5.

Huarte, M. (2015). The emerging role of lncRNAs in cancer. Nat. Med. *21*, 1253–1261.

Jacques, C., Calleja, L.R., Baud'Huin, M., Quillard, T., Heymann, D., Lamoureux, F., and Ory, B. (2016). MiRNA-193a-5p repression of p73 controls Cisplatin chemoresistance in primary bone tumors. OncoTarget *7*, 54503–54514.

Jiang, X., and Li, H. (2018). MiR-1180-5p regulates apoptosis of Wilms' tumor by targeting *p73*. OncoTargets Ther. *11*, 823–831.

Jost, C.A., Marin, M.C., and Kaelin, W.G., Jr. (1997). p73 is a simian [correction of human] p53-related protein that can induce apoptosis. Nature *389*, 191–194.

Kogo, R., Shimamura, T., Mimori, K., Kawahara, K., Imoto, S., Sudo, T., Tanaka, F., Shibata, K., Suzuki, A., Komune, S., et al. (2011). Long noncoding RNA HOTAIR regulates polycomb-dependent chromatin modification and is associated with poor prognosis in colorectal cancers. Cancer Res. *71*, 6320–6326.

Kotulak, A., Wronska, A., Kobiela, J., Godlewski, J., Stanislawowski, M., and Wierzbicki, P. (2016). Decreased expression of p73 in colorectal cancer. Folia Histochem. Cytobiol. *54*, 166–170.

Li, J., Chen, Z., Tian, L., Zhou, C., He, M.Y., Gao, Y., Wang, S., Zhou, F., Shi, S., Feng, X., et al. (2014). LncRNA profile study reveals a three-lncRNA signature associated with the survival of patients with oesophageal squamous cell carcinoma. Gut *63*, 1700–1710.

Li, M., Qian, X., Zhu, M., Li, A., Fang, M., Zhu, Y., and Zhang, J. (2018). miR-1273g-3p promotes proliferation, migration and invasion of LoVo cells via cannabinoid receptor 1 through activation of ERBB4/PIK3R3/mTOR/S6K2 signaling pathway. Mol. Med. Rep. *17*, 4619–4626.

Liu, Z., Shao, Y., Tan, L., Shi, H., Chen, S., and Guo, J. (2014). Clinical significance of the low expression of FER1L4 in gastric cancer patients. Tumour Biol. *35*, 9613–9617.

Loewen, G., Jayawickramarajah, J., Zhuo, Y., and Shan, B. (2014). Functions of lncRNA HOTAIR in lung cancer. J. Hematol. Oncol. *7*, 90.

Logotheti, S., Pavlopoulou, A., Galtsidis, S., Vojtesek, B., and Zoumpourlis, V. (2013). Functions, divergence and clinical value of TAp73 isoforms in cancer. Cancer Metastasis Rev. *32*, 511–534.

Melino, G., De Laurenzi, V., and Vousden, K.H. (2002). p73: friend or foe in tumorigenesis. Nat. Rev. Cancer *2*, 605–615.

Napoli, M., and Flores, E. (2017). The p53 family orchestrates the regulation of metabolism: physiological regulation and implications for cancer therapy. Br. J. Cancer *116*, 149–155.

Naz, F., Tariq, I., Ali, S., Somaida, A., Preis, E., and Bakowsky, U. (2021). The role of long non-coding RNAs (lncRNAs) in female oriented cancers. Cancers (Basel) *13*, 6102.

Nicolai, S., Rossi, A., Di Daniele, N., Melino, G., Annicchiarico-Petruzzelli, M., and Raschellà, G. (2015). DNA repair and aging: the impact of the p53 family. Aging *7*, 1050–1065.

Niu, X., Fu, N., Du, J., Wang, R., Wang, Y., Zhao, S., Du, H., Wang, B., Zhang, Y., Sun, D., et al. (2016). miR-1273g-3p modulates activation and apoptosis of hepatic stellate cells by directly targeting PTEN in HCV-related liver fibrosis. FEBS Lett. *590*, 2709–2724.

Ory, B., Ramsey, M.R., Wilson, C., Vadysirisack, D.D., Forster, N., Rocco, J.W., Rothenberg, S.M., and Ellisen, L.W. (2011). A microRNA-dependent program controls p53-independent survival and

chemosensitivity in human and murine squamous cell carcinoma. J. Clin. Invest. *121*, 809–820.

Ozaki, T., Kubo, N., and Nakagawara, A. (2010). p73-Binding partners and their functional significance. Int. J. Proteomics *2010*, 283863.

Park, J., and Schwarzbauer, J.E. (2014). Mammary epithelial cell interactions with fibronectin stimulate epithelial-mesenchymal transition. Oncogene *33*, 1649–1657.

Qiao, Q., and Li, H. (2016). LncRNA FER1L4 suppresses cancer cell proliferation and cycle by regulating PTEN expression in endometrial carcinoma. Biochem. Biophys. Res. Commun. *478*, 507–512.

Rinn, J.L., and Chang, H.Y. (2012). Genome regulation by long noncoding RNAs. Annu. Rev. Biochem. *81*, 145–166.

Satija, Y.K., and Das, S. (2016). Tyr99 phosphorylation determines the regulatory milieu of tumor suppressor p73. Oncogene *35*, 513–527.

Shao, Y., Chen, H., Jiang, X., Chen, S., Li, P., Ye, M., Li, Q., Sun, W., and Guo, J. (2014). Low expression of lncRNA-HMlincRNA717 in human gastric cancer and its clinical significances. Tumour Biol. *35*, 9591–9595.

Song, H., Sun, W., Ye, G., Ding, X., Liu, Z., Zhang, S., Xia, T., Xiao, B., Xi, Y., and Guo, J. (2013). Long non-coding RNA expression profile in human gastric cancer and its clinical significances. J. Transl. Med. *11*, 225.

Stiewe, T., Zimmermann, S., Frilling, A., Esche, H., and Pützer, B.M. (2002). Transactivation-deficient DeltaTA-p73 acts as an oncogene. Cancer Res. *62*, 3598–3602.

Struhl, K. (2007). Transcriptional noise and the fidelity of initiation by RNA polymerase II. Nat. Struct. Mol. Biol. *14*, 103–105.

Tang, J.Y., Lee, J.C., Chang, Y.T., Hou, M.F., Huang, H.W., Liaw, C.C., et al. (2013). Long noncoding RNAs-related diseases, cancers, and drugs. Sci. World J. *2013*, 943539.

Uboveja, A., Satija, Y.K., Siraj, F., and Saluja, D. (2020). p73 – NAV3 axis plays a critical role in suppression of colon cancer metastasis. Oncogenesis *9*, 12.

Vleminckx, K., Vakaet, L., Mareel, M., Fiers, W., and Van Roy, F. (1991). Genetic manipulation of E-cadherin expression by epithelial tumor-cells reveals an invasion suppressor role. Cell *66*, 107–119.

Vu, T., and Datta, P.K. (2017). Regulation of EMT in colorectal cancer: a culprit in metastasis. Cancers (Basel) *16*, 171.

Wapinski, O., and Chang, H.Y. (2011). Long noncoding RNAs and human disease. Trends Cell Biol. *21*, 354–361.

Wu, J., Huang, J., Wang, W., Xu, J., Yin, M., Cheng, N., and Yin, J. (2017). Long non-coding RNA Fer-1-like protein 4 acts as a tumor suppressor via miR-106a-5p and predicts good prognosis in hepatocellular carcinoma. Cancer Biomark. *19*, 55–65.

Xia, T., Chen, S., Jiang, Z., Shao, Y., Jiang, X., Li, P., Xiao, B., and Guo, J. (2015). Long noncoding RNA *FER1L4* suppresses cancer cell growth by acting as a competing endogenous RNA and regulating *PTEN* expression. Sci. Rep. *5*, 13445.

Xu, C., Shao, Y., Xia, T., Yang, Y., Dai, J., Luo, L., Zhang, X., Sun, W., Song, H., Xiao, B., and Guo, J. (2014). lncRNA-AC130710 targeting by miR-129-5p is upregulated in gastric cancer and associates with poor prognosis. Tumour Biol. *35*, 9701–9706. https://doi.org/10.1007/s13277-014-2274-5.

Yang, F., Huo, X.S., Yuan, S.X., Zhang, L., Zhou, W.P., Wang, F., and Sun, S.H. (2013). Repression of the long noncoding RNA-LET by histone deacetylase 3 contributes to hypoxia-mediated metastasis. Mol. Cell *28*, 1083–1096.

Yang, F., Zhang, L., Huo, X.S., Yuan, J.H., Xu, D., Yuan, S.X., Zhu, N., Zhou, W.P., Yang, G.S., Wang, Y.Z., et al. (2011). Long noncoding RNA high expression in hepatocellular carcinoma facilitates tumor growth through enhancer of zeste homolog 2 in humans. Hepatology *54*, 1679–1689.

Yoon, J.H., Abdelmohsen, K., and Gorospe, M. (2013). Posttranscriptional gene regulation by long noncoding RNA. J. Mol. Biol. *425*, 3723–3730.

Yoon, M.K., Ha, J.H., Lee, M.S., and Chi, S.W. (2015). Structure and apoptotic function of p73. BMB Rep. *48*, 81–90.

Yue, B., Sun, B., Liu, C., Zhao, S., Zhang, D., Yu, F., and Yan, D. (2015). Long non-coding RNA Fer-1-like protein 4 suppresses oncogenesis and exhibits prognostic value by associating with miR-106a-5p in colon cancer. Cancer Sci. *106*, 1323–1332.

Zhang, F., Zhang, L., and Zhang, C. (2016). Long noncoding RNAs and tumorigenesis: genetic associations, molecular mechanisms, and therapeutic strategies. Tumour Biol. *37*, 163–175.

STAR★METHODS

KEY RESOURCES TABLE

REAGENT or RESOURCE	IDENTIFIER	SOURCE
Antibodies		
anti-p73	Santacruz	Cat# sc-7957; RRID:AB_2207314
anti-p73	Abcam	Cat# ab14430; RRID:AB_301211
anti-β-actin	Santacruz	Cat# sc-47778; RRID:AB_626632
anti-Fibronectin	Santacruz	Cat# sc-8422; RRID:AB_627598
anti-E-cadherin	Abcam	Cat# ab40772; RRID:AB_731493
anti-SNAIL	Abcam	Cat# ab85936; RRID:AB_1925448
anti-N-cadherin	Abcam	Cat# ab76011; RRID:AB_1310479
anti-Vimentin	Abcam	Cat#ab92547; RRID:AB_10562134
Oligonucleotides		
p73 FP:5′ GCACCACGTTT GAGCACCTCT 3′	IDT	N/A
p73 RP:5′ GCAGATTGAA CTGGGCCATGA 3′	IDT	N/A
β-actin FP:5′ CCCTGGACTTC GAGCAAGAGAT 3′	IDT	N/A
β-actin RP:5′ AAGGTAGTTT CGTGGATGCCACA 3′	IDT	N/A
p73 shRNA:FP:5′ TCGAGGTCCGCCAAG GGTTACAGAGCATTTATT CAAGAGATAAATGCTCTGT AACCCTTGGCGGACC 3′	IDT	N/A
RP:5′ GATCC AAAAAGCCAAGGGT TACAGAGCATTTATC TCTTGAATAAATGCTCTG TAACCCTTGGCGGACC 3′	IDT	N/A
Primer: U1 region FP:5′ CATTAGCCA GGTATGGTGGTGC 3′	IDT	N/A
RP:5′ GGAGGCAGAAGT TGCAGTGAAG 3′	IDT	N/A
Primer: U2 region FP:5′ CCTGACCCT TTCTGCTCTCA 3′	IDT	N/A
RP:5′GGAAGCCAG GTGTCCTTAAC 3′	IDT	N/A
Primer: U3 region FP:5′ TCTACCATG TGCCAAACCCT 3′	IDT	N/A
RP:5′CCTCCCACAC AGCTGAGATT 3′	IDT	N/A
Primer: D1 region FP:5′ GGGCTTTGG ATTGGAGTTTA 3′	IDT	N/A

(Continued on next page)

Continued

REAGENT or RESOURCE	IDENTIFIER	SOURCE
RP:5′ CAGACGGGAAATGGCAGAT 3′.	IDT	N/A
Primer: D2 region		
FP:5′ GCTGAGCAATG AGGATTCCG -3′	IDT	N/A
RP:5′ CGGAATCCTCA TTGCTCAGC -3′	IDT	N/A
ChIP Primers: BSS1 FP:5′ ATCACACC ATGCACTCCAA 3′	IDT	N/A
BSS1 RP:5′ GGCCTGAA CACAAGGAATGT 3′	IDT	N/A
BSS2 FP:5′ TGTGATTCC CCTCTCTCTGG 3′	IDT	N/A
BSS2 RP:5′ TTCCTGACTCA GCCTCCCTA3′	IDT	N/A
β-actin FP:5′ CACCATTGGCA ATGAGCGGTTC 3′	IDT	N/A
β-actin RP:5′ AGGTCTTTGC GGATGTCCACGT 3′	IDT	N/A
p21 FP:5′ GTGGCTCTG ATTGGCTTTCTG 3′	IDT	N/A
p21 RP:5′ CTGAAAACAG GCAGCCCAAG 3′	IDT	N/A
Chemicals		
Etoposide	Sigma	Cat# E1383
Puromycin	Sigma	Cat# P8833
Dulbecco's Modified Eagle's Medium (DMEM)	Invitrogen	Cat# 11965118
Fetal Bovine Serum	GIBCO	Cat# 10270106
Penicillin-Streptomycin	Invitrogen	Cat# 15140122
Lipofctamine-2000	Sigma	Cat# 11668030
SYBR-Green	Promega	Cat# A6001
Critical commercial assays		
Dual-Luciferase Reporter Assay System	Promega	Cat# E1910
RNeasy Mini Kit	QIAGEN	Cat# 74104
Q5-Site Directed Mutgenesis Kit	NEB	Cat# E0554S
High-capacity cDNA RT Kit	Applied Biosystems	Cat# 4368814
QuantiGene ViewRNA ISH Cell Assay	Thermo Fischer Scientific	QVC0001
ViewRNA ISH Tissue Assay	Invitrogen	Cat#19931
DeadEnd Fluorometric TUNEL system	Promega	Cat#G3250
Annexin V Apoptosis Detection Kit FITC	Thermo Fischer Scientific	Cat#88-8005-72
Edu Proliferation Kit (iFluor 488)	Abcam	Cat#ab219801
Softwares		
GraphPad Prism	v.5.0c	RRID:SCR_002798
ImageJ	v.149	RRID:SCR_003070

RESOURCE AVAILABILITY

Lead contact

Daman Saluja (dsalujach1959@gmail.com)

Materials availability

Plasmids generated in this study are available upon request from the lead contact, Daman Saluja (dsalujach1959@gmail.com).

Data and code availability

- All data produced in this study are included in the published article and its supplemental information, or are available from the lead contact upon request

- For each analysis performed, the software and version used have been detailed in the key resources table

- This report does not report original code

- Any additional information required to reanalyze the data reported in this paper is available from the lead contact upon request

EXPERIMENTAL MODEL AND SUBJECT DETAILS

Tissue samples

30 paraffin-embedded biopsy proven colorectal carcinoma tissue samples were obtained from the archives of National Institute of Pathology, Safdarjung Hospital, New Delhi to analyse the mRNA expression of p73 and FER1L4 by RNA – *In situ* hybridization (ISH) technique. As no previous report was available, 30 clinical samples for preliminary experiment were chosen by convention. Only retrospective metastatic and non-metastatic biopsy samples were considered in the inclusion criteria. The awareness of the metastatic and non-metastatic samples was restricted to the clinician and the results were compared only after RNA-ISH was performed. This study was approved by the Ethical Review Board of National Institute of Pathology, Safdarjung Hospital (Reference number: NIP-IEC/14-06-18/03) and Dr.B.R. Ambedkar Centre for Biomedical Research, University of Delhi (Reference number: ACBR/IHEC/DS-03/09-18).

Cell lines

HCT116p53$^{-/-}$ and HCT116p53$^{+/+}$ cell lines were a kind gift from the lab of Bert Vogelstein, Johns Hopkins University, Maryland, US. The cell lines were maintained in Dulbecco Modified Eagle's Medium (DMEM) complete with fetal bovine serum (Invitrogen) and 100 U/mL Penicillin Streptomycin at 37°C in humidified air with 5% CO_2. They were frequently examined for mycoplasma contamination. HCT116p53$^{-/-}$p73kd cell line was created by transfecting pBABEU6 vector containing shRNA against p73 and puromycin-resistant cells were selected. The sequences used for shRNA are as follows: TAp73 (5′ - GGCATGACTACATCA - 3′), scrambled for TAp73 (5′ - GCCAGACTCGTTTACATGA - 3′). HCT116p53$^{-/-}$FER1L4kd cell line was created by transfecting four siRNA's (Qiagen, Catalogue number-1027418) against FER1L4. HCT116p53$^{+/+}$p73kd cell line was created by transfecting pBABEU6 vector containing shRNA against p73 and puromycin-resistant cells were selected for further study. Every transfection was performed using Lipofectamine 2000 (Invitrogen) as per manufacturer's protocol. Cells were permitted to grow to ~50% confluency prior to treatment with etoposide (Sigma) for the indicated time periods.

METHOD DETAILS

Plasmids and shRNA

For luciferase reporter experiments, the promoter region of FER1L4; region U1 (nucleotides −4002/−3107 from the TSS), region U2 (nucleotides −2539/−1825 from the TSS), region U3 (nucleotides −1680/−844 from the TSS), region D1 (nucleotides +1092/+1691) and region D2 (nucleotides +2116/+2900 from the TSS) were cloned in pGL4.20 vector (Promega). To obtain an FER1L4 expression vector, a full-length FER1L4 DNA fragment was amplified by polymerase chain reaction (PCR) using Taq polymerase. The reaction steps were as follows: 94°C for 5 min; 94°C for 45 sec; 60°C for 45 sec; 72°C for 1 min, for a total of 30 cycles and 72°C for 10 min. The primer sequences for FER11L4 were: Forward, 5′-GATTCAGGT GGGCGGGCTGGTG-3′ and reverse, 5′-TCAGTGGCTGTGATAGGTTTA-3′. The PCR products were inserted into mammalian expression vector pCDH-CB-IRES-copGFP-T2A-Puro overexpression vector (Addgene, Plasmid #72299) and the constructed pCDH-FER1L4 overexpression plasmid was transfected

into cells. The transfected cells were selected using puromycin. In a similar manner, a p73 overexpression plasmid was created by cloning full length p73 DNA fragment in Pgex-4T-1 over-expression plasmid and selection was done using puromycin. Putative miR-1273g-3p binding sites in FER1L4, both wild-type (WT) and mutant (MU), were synthesized and cloned downstream of the luciferase gene in pmirGLO dual-luciferase miRNA Target Expression Vector. The primers, miR1273g-3p mimic, miR-NC mimic and shRNA utilized for cloning are mentioned in key resources table.

Luciferase assays

Cells were seeded in a 12 well plate and grown overnight. The different FER1L4 promoter constructs (500 ng) were co-transfected with Renilla luciferase construct pRL-TK (500 ng) using Lipofectamine 2000 reagent (Thermo Fischer Scientific) as per manufacturer's protocol. Cells were exposed to etoposide (20 μM) treatment six hours post-transfection. After incubation for 24 hours, cells were given two washes with PBS and lysed in passive lysis buffer (300 μL/well) supplied by the Dual-Luciferase Reporter Assay System (Promega). The lysate was used to analyze firefly and renilla luciferase activities using luminometer. Firefly luciferase values were then normalized to Renilla luciferase. The error bars indicate mean $\pm$ SD of three independent experiments conducted.

Cell counting kit 8 (CCK-8) assay

Measurement of cell viability was conducted by Cell Counting Kit-8 (DojinDO, Japan) assay. Briefly, 1×10^3 transfected cells were seeded into a 96-well plate. CCK-8 solution (10 μL) was added into each well at different time points (24 h, 48 h and 72 h), for an additional 4 hours at 37°C. The absorbance value was calculated in a microplate reader at 450nm wavelength.

Ethynyldeoxyuridine (EdU) assay

Cell proliferation was measured by EdU assay kit (Abcam) as per manufacturer's instructions. Cells were seeded in 6-well plates on a coverslip at a density of 5×10^3 cells per well post-transfection. Following this, the cells were treated with 20 μM EdU labelling medium and were cultured at 37°C under 5% CO_2 for 4 hours. The cultured cells were fixed for 30 min with 4% paraformaldehyde (pH= 7.4). Cells were then washed and treated with permeabilization buffer for 20 min at RT. EdU reaction cocktail (200 μL) was then added to react with EdU for 30 min followed by addition of Hoechst 33342 (100 μL) to the cells. Fluorescent microscopy was utilized to analyze the percentage of EdU positive cells in five random fields per well.

Cell cycle analysis

The transfected cells at 60% confluency were serum deprived for 24 hours. The G0 phase synchronous cell population thus procured was subjected to etoposide (20 μM) treatment for various time points. Post the required time interval, cells were washed with cold PBS, centrifuged and fixed in 70% (v/v) ethanol at 4°C. Ethanol was then removed by washing the cells with cold PBS twice. Following this, cells were treated with PBS containing RNaseA (0.005 mg/mL) at 37°C for 30 min. Cells were then treated with propidium iodide (PI) (0.1 mg/mL) and incubated in dark for 15 min at room temperature. The cells distribution in different phases of the cell cycle was measured on FACScalibur using CellQuestPro software (Becton Dickinson, USA).

QuantiGene ViewRNA ISH cell assay

$HCT116p53^{-/-}p73^{+/+}$ (Control) and $HCT116p53^{-/-}p73^{+/+}FER1L4kd$ (FER1L4kd) cells were seeded (0.1 million) onto cover slips in 6-well plates. The cells were subjected to etoposide (20 μM) treatment for 24 hours and then fixed with 4% formaldehyde. The cells were then permeabilized with protease solution, followed by incubation with label probes against FER1L4 for 3 hours at 40°C. The cells are then treated with pre-amplifier mix, amplifier mix and label probe according to the manufacturer's protocol. Finally the cells were stained with DAPI and viewed by fluorescent microscopy.

Terminal deoxynucleotidyltransferase dUTP nick end labelling (TUNEL) assay

DNA fragmentation caused by endonucleases is one of the events that occur during apoptosis resulting in the formation of multiple 3' hydroxyl ends. These ends are labelled with fluorescein-12-dUTP at 3'- OH DNA ends using Terminal Deoxynucleotidyl Transferase (TdT) and are identified directly by fluorescent microscopy. Staining was performed as per the manufacturer's instructions (Promega).

Chromatin immunoprecipitation (ChIP) assays

HCT116p53$^{-/-}$ and HCT116p53$^{-/-}$p73kd cells subjected to etoposide (20 μM) treatment for 24 hours were cross-linked using 1% formaldehyde for 10 minutes, exposed to 10X Glycine for 5 minutes, washed with PBS and lysed by ChIP lysis buffer. Following this, the lysate was sonicated by QSonicator to shear the DNA into fragments of size nearly 200–1000 bp. Anti-p73 or control IgG antibodies were added to the lysate and incubated at 4°C overnight followed by treatment with fresh Protein A agarose slurry for 1 h. Prior to immunoprecipitation, 1% of the supernatant was separated to be used as "input." Precipitated chromatin complexes were detached from the beads by treatment with 200 μL of elution buffer (20% SDS, 1M NaHCO$_3$) for 30 mins. 5 M NaCl was used to reverse the protein-DNA cross-links at 65°C for 4–5 hours and immunoprecipitated DNA was quantified by qPCR using primers bordering the p73 binding site BS1; BSS1 (−3781 to −3761) present in U1 region of FER1L4 promoter and primers bordering the p73 binding site BS2; BSS2 (−2381 to −2362) present in U2 region of FER1L4 promoter. Primer sequences used are mentioned in the key resources table.

RNA immunoprecipitation assay

HCT116p53$^{-/-}$ and HCT116p53$^{-/-}$p73kd cells subjected to etoposide (20 μM) treatment for 24 hours were cross-linked using 1% formaldehyde for 10 minutes. Cells were harvested by using nuclear isolation buffer and were kept on ice for 20 mins. Nuclei was pelleted by centrifugation at 2500g for 15 minutes. The pellet was resuspended in freshly prepared RIP buffer (1 mL). Some portion was separated to be used as mock. The chromatin so obtained was sheared by QSonicator. Th nuclear membrane and debris was pelleted by centrifugation at 13,000 rpm for 10 minutes. Anti-p73 antibody was added to the supernatant (6–10 mg) and incubated overnight at 4 °C. Following this, protein A/G beads were added to the complex and incubated for 1 hour at 4°C with gentle rotation. The beads were pelleted at 2500 rpm for 30 seconds and the supernatant was removed. The beads were resuspended in 500μL of RIP buffer and the washes were repeated thrice, followed by one wash with PBS. The co-precipitated RNA was isolated by resuspending the beads in TRIZOL RNA extraction reagent according to manufacturer's instructions. The RNA was eluted in nuclease-free water (20 μL). RT-qPCR was carried out as the end-point experiment.

Site-directed mutagenesis assay

Q5 Site-Directed Mutagenesis Kit (New England Biolabs) was used to mutate specific nucleotides. NEBase-Changer tool was used to design primers carrying mutated nucleotides and PCR was performed using the designed primers and master mix solution of Q5 Hot Start High-Fidelity DNA polymerase. Post-PCR, the amplified product was subjected to treatment with a Kinase-Ligase-Dpn1 (KLD) enzyme mixture for 5 minutes at room temperature. The product was transformed in high-efficiency NEB 5-alpha competent *E.coli* cells. Finally, positive site-directed mutagenesis was confirmed by sending the constructs for DNA sequencing (Pragati Biomedicals).

Annexin-V/propidium iodide assay

HCT116p53$^{-/-}$p73$^{+/+}$, HCT116p53$^{-/-}$FER1L4kd and HCT116p53$^{-/-}$p73kd cells were subjected to etoposide (20 μM) treatment for the required time interval. Cells were then treated with APC (allophycocyanin) labelled annexin-V and PI according to the manufacturer's instructions (eBiosciences, USA). Cell population was measured for distribution in different apoptotic phases by FACScalibur utilizing CellQuestPro software (Becton Dickinson, USA).

Western blotting analysis

Cell lysis buffer for lysis of cells was prepared as follows: (1M Tris-HCl pH 8, 5M NaCl, 0.5M EDTA, 3% Na$_4$P$_2$O$_7$, 10% NP40, 1M NaF, 200mM PMSF, 1X Protease inhibitor cocktail; Roche, Basel, Switzerland). Pierce BCA Protein Assay Kit (Thermo Fisher Scientific) was used to measure the concentration of the samples for equal loading. Bovine Albumin Serum (BSA, Invitrogen) was utilized to devise a standard curve for protein concentration. Uniform amount of protein per sample was loaded to SDS-PAGE and transferred to a PVDF membrane (Millipore). The membrane was treated with the antibody of interest at 4°C overnight in 5% BSA solution or 5% skimmed milk solution. The blots were exposed to HRP-conjugated secondary antibodies (Santacruz) at room temperature for 45 minutes, followed by ECL-based detection (Bio-Rad).

Migration assay measured using calcein-AM

Cells were serum starved for 24 hours prior to assay. Then the cells were centrifuged at 250 X g for 10 minutes, following which the supernatant was removed and washed with 1X wash buffer. The cell pellet was resuspended at 1×10^6 cells/mL in a serum free medium. Cells (0.1×10^6 cell/ insert) were seeded in the top compartment of Trevigen's Cultrex 24 well Cell Migration Plate, which makes use of a simplified Boyden chamber design consisting of an 8 μm pore size polyethylene terephthalate (PET) membrane. 500 μL of complete media was poured into the bottom chamber and the whole apparatus was assembled and incubated at 37 ºC in a CO_2 incubator for 36 hours. Post 36 hours, the top and the bottom chambers were cleared and washed with 1X wash buffer. Cell migration was measured by Calcein-AM. Cell Dissociation Solution/Calcein-AM was next added to the lower chamber and the plate was read at 485 nm excitation, 520 nm emission.

Invasion assay measured using Calcein-AM

Trevigen's Culture Coat 24 well BME (Basement membrane Extract) coated Cell Invasion Chambers were used to measure the cells's invasive ability. 10% FBS was added as a chemo-attractant to the bottom chamber. Serum-starved cells for 24 hours were used for this assay. Cells (0.1×10^6 cells/insert) were plated in the top chamber and treated with etoposide (20 μM) for 36 hours. The cells that migrated to the lower chamber were measured using Calcein-AM present in the Cell Dissociation Solution. The percentage of invading cells was measured by reading the plate at 485 nm excitation, 520 nm emission.

Wound-healing assay

Cells were plated in 24 well plates using 1% FBS-containing DMEM media. Post 24 hours of plating, a wound was fashioned using a cell scratcher. The media in the plate was replaced with media containing etoposide (20 μM). Images of the scratched area were recorded quickly after the scratch and then after 12 hours, 24 hours and 36 hours using a phase-contrast microscope at 10X magnification. The area of wound was measured by Java's Image J software (http://rsb.info.nih.gov). The migration of cells toward the wound area was expressed as percentage of wound closure:

$$\% \text{ of wound closure} = [(A_{t=0 \text{ h}} - A_{t=\Delta \text{ h}} / A_{t=0 \text{ h}})] \times 100\%,$$

where $A_{t=0h}$ is the area of wound measured immediately after scratching, and $A_{t=\Delta h}$ is the area of wound measured 12 or 24 h after scratching.

RNA extraction and qRT-PCR

Qiagen's RNA extraction kit was utilized to extract total RNA from the cells. cDNA synthesis kit (Applied Biosystems) was used to synthesize cDNA as per the manufacturer's protocol. Quantitative PCR (qPCR) was performed for the respective genes by using validated qPCR primers (IDT) and SYBR Green mastermix (Promega) in BioRad S-1000 Thermo cycler. For internal control, β-actin was chosen. To detect the levels of miR-1273g-3p, a taqman probe specific to miR-1273g-3p (5′ - ACCACUGCACUCCAGCCUGAG-3′) was designed and RNU6B (5′- CGCAAGGATGACACGCAAATTCGTGAAGCGTTCCATATTTTT-3′) was used as endogenous control. Primers used in the study are mentioned in key resources table. The ΔΔCt method was utilized to measure the abundance of RNA for each gene as compared to β-actin expression. Error bars are representative of mean $\pm$ SD of three independent experiments.

RNA-*In situ* hybridization (RNA-ISH)

Tissue sections (5 μm) were deparaffinized, followed by rehydration in graded alcohols and processed using the ViewRNA ISH Tissue Assay (Invitrogen) procedure. In a nutshell, the sections were subjected to antigen retrieval at 60°C for 60 mins in 1X Pretreatment solution. The tissue sections were then treated with protease digestion and then fixed with 10% NBF. Slides were subsequently incubated with ViewRNA Type 1 Probe set (p73 and FER1L4) block for 2 hours at 40°C. The sections were then treated with pre-amplifier, amplifier and label probe to detect the primary probe. Samples were incubated with Fast Red Substrate for 30 mins at 40°C, followed by counterstaining with hematoxylin. Results were recorded by calculating the percentage of tumor cells portraying distinctive nuclear and cytoplasmic staining. Immunoreactivity for p73 and FER1L4 in non-metastatic and metastatic colorectal cancer tissues was scored as follows: None (<5%, score 0), Weak (+, 5%-25%, score 1), Moderate (++, 25%-75%, score 2), Intense (+++, >75%, score 3).

CellPress
OPEN ACCESS

QUANTIFICATION AND STATISTICAL ANALYSIS

Statistics

Every statistical analysis was conducted using Prism software (Graphpad Prism5). All data are expressed as mean $\pm$ (SD) of atleast three independent experiments. Two-tailed Student's t–test was utilized for calculating significance between two groups. A one way analysis of variance was utilized in case of multiple group testing. A two-tailed value of $p < 0.05$ was considered statistically significant and $*p < 0.05$, $**p < 0.01$, $***p < 0.001$. The statistical significance of p73 and FER1L4 expression were analysed by Pearson χ^2 test.